

1 **An oligomeric state-dependent switch in FICD regulates**
2 **AMPylation and deAMPylation of the chaperone BiP**

3

4 Luke A. Perera¹, Claudia Rato¹, Yahui Yan¹, Lisa Neidhardt¹, Stephen H. McLaughlin²,
5 Randy J. Read¹, Steffen Preissler^{1*}, David Ron^{1*}.

6

7 1 Cambridge Institute for Medical Research, University of Cambridge, Cambridge
8 CB2 0XY, United Kingdom.

9 2 MRC Laboratory of Molecular Biology, Francis Crick Avenue, Cambridge CB2
10 0QH, United Kingdom.

11 * Address correspondence to: David Ron: dr360@medschl.cam.ac.uk, Phone +44
12 (0)1223 768 940, or Steffen Preissler: sp693@cam.ac.uk

13

14

15 **Impact Statement**

16

17 Unique amongst known chaperones, the endoplasmic reticulum (ER)-localized
18 Hsp70, BiP, is subject to transient inactivation under conditions of low ER stress
19 by reversible, covalent modification – AMPylation. The enzyme responsible for
20 this modification, FICD, is in fact a bifunctional enzyme with a single active site
21 capable of both AMPylation and deAMPylation. Here we elucidate, by
22 biochemical, biophysical and structural means, the mechanism by which this
23 enzyme is able to switch enzymatic modality: by regulation of its oligomeric
24 state. The oligomeric state-dependent reciprocal regulation of FICD activity is, in
25 turn, sensitive to the ATP/ADP ratio. This allosteric pathway potentially
26 facilitates the sensing of unfolded protein load in the ER and permits the
27 transduction of this signal into a post-translational buffering of ER chaperone
28 activity.

29 **Abstract**

30

31 AMPylation is an inactivating modification that matches the activity of the major
32 endoplasmic reticulum (ER) chaperone BiP to the burden of unfolded proteins. A single
33 ER-localised Fic protein, FICD (HYPE), catalyses both AMPylation and
34 deAMPylation of BiP. However, the basis for the switch in FICD's activity is unknown.
35 We report on the transition of FICD from a dimeric enzyme, that deAMPylates BiP, to
36 a monomer with potent AMPylation activity. Mutations in the dimer interface or in
37 residues tracing an inhibitory relay from the dimer interface to the enzyme's active site
38 favour BiP AMPylation in vitro and in cells. Mechanistically, monomerisation relieves
39 a repressive effect allosterically-propagated from the dimer interface to the inhibitory
40 Glu234, thereby permitting AMPylation-competent binding of MgATP. Whereas, a
41 reciprocal signal propagated from the nucleotide binding site, provides a mechanism
42 for coupling the oligomeric-state and enzymatic activity of FICD to the energy status
43 of the ER.

44

45 (148 Words)

46

47 **Introduction**

48 In all domains of life, protein folding homeostasis is achieved by balancing the burden
49 of unfolded proteins and the complement of chaperones. In the endoplasmic reticulum
50 (ER) of animal cells, this match is facilitated by the unfolded protein response (UPR).
51 In addition to well-recognized transcriptional and translational strands of the UPR
52 (Walter & Ron, 2011), recent findings have drawn attention to the existence of rapid
53 post-translational mechanisms that adjust the activity of the ER Hsp70 chaperone BiP.
54 Best understood amongst these is AMPylation, the covalent addition of an AMP moiety
55 from ATP onto a hydroxyl group-containing amino acid side chain.

56 AMPylation conspicuously occurs on Thr518 of BiP (Preissler *et al*, 2015b; Broncel *et*
57 *al*, 2016; Casey *et al*, 2017). The resulting BiP-AMP is locked in a domain-coupled
58 ATP-like state (Preissler *et al*, 2015b, 2017b; Wieteska *et al*, 2017). Consequently, BiP-
59 AMP has high rates of client protein dissociation (Preissler *et al*, 2015b). Moreover,
60 the ATPase activity of BiP-AMP is resistant to stimulation by J-protein co-factors,
61 which greatly reduces the chaperone's ability to form high-affinity complexes with its
62 clients (Preissler *et al*, 2017b). AMPylation therefore serves to inactivate BiP. This
63 modification is temporally dynamic and the levels of BiP-AMP respond to changes of
64 the protein folding load in the ER.

65 Consistent with its inactivating character, BiP modification in cells is enhanced by
66 inhibition of protein synthesis (Laitusis *et al*, 1999) or during recovery from ER stress;
67 when BiP levels exceed the requirements of unfolded client proteins (Preissler *et al*,
68 2015b). Conversely, as levels of ER stress increase, modification is reversed by
69 deAMPylation, recruiting BiP back into the chaperone cycle (Laitusis *et al*, 1999;
70 Chambers *et al*, 2012; Preissler *et al*, 2015b). Accordingly, BiP modification creates a
71 readily-accessible pool of latent folding capacity that buffers both ER stress (through
72 deAMPylation) and over-chaperoning (through AMPylation). These features may
73 contribute to the observation whereby in the *Drosophila* visual system, loss of the
74 ability to AMPylate BiP results in light-induced blindness (Rahman *et al*, 2012;
75 Moehlman *et al*, 2018).

76 AMPylation of BiP is mediated by the ER-localised enzyme FICD (filamentation
77 induced by cAMP domain protein, also known as HYPE) (Ham *et al*, 2014; Sanyal *et*
78 *al*, 2015; Preissler *et al*, 2015b). FICD is the only known metazoan representative of a
79 large family of bacterial Fic-domain proteins (Khater & Mohanty, 2015a). Fic proteins

80 contain a conserved active site motif, HPF_x(D/E)GN(G/K)R_{1xx}R₂, and many possess
81 a glutamate-containing inhibitory alpha helix (α_{inh}) responsible for auto-inhibition of
82 their canonical AMPylation activity (Engel *et al*, 2012; Goepfert *et al*, 2013). FICD is
83 a class II Fic protein (with its α_{inh} N-terminal to its Fic domain) and an ER-localised
84 type II, single-pass transmembrane protein, with a short cytoplasmic portion and a large
85 luminal-facing catalytic domain (Worby *et al*, 2009; Bunney *et al*, 2014).

86 Crystal structures of FICD and other Fic domain proteins suggest that engagement of
87 Glu234 (of the α_{inh}) with Arg374 (R₂ of the Fic motif) prevents binding of MgATP in
88 a conformation conducive to catalysis (Engel *et al*, 2012; Goepfert *et al*, 2013; Bunney
89 *et al*, 2014; Truttmann *et al*, 2016). Moreover, in vitro, modification of BiP by purified
90 FICD requires mutation of Glu234; an observation suggesting that an AMPylation
91 repressed state is favoured by wild-type FICD. Remarkably, the Fic domain of FICD is
92 also responsible for BiP deAMPylation; an activity that depends on Glu234 (Preissler
93 *et al*, 2017a; Casey *et al*, 2017) and magnesium (Veyron *et al*, 2019). These findings
94 point to deAMPylation as the default activity of the bifunctional enzyme and implicate
95 Glu234 in a functional switch between the two antagonistic activities of the Fic active
96 site.

97 The Fic domain of human FICD forms a stable back-to-back asymmetric dimer via two
98 dimerisation surfaces (Bunney *et al*, 2014; Truttmann *et al*, 2016) and a monomerising
99 mutation in the dimer interface of *Drosophila* FICD did not block BiP deAMPylation
100 in vitro (Casey *et al*, 2017). Nonetheless, distantly related bacterial enzymes hint at a
101 possible regulatory role for Fic dimerisation: a mutation in *Clostridium difficile* Fic
102 (CdFic) dimer interface increased auto-AMPylation (Dedic *et al*, 2016) and changes in
103 oligomeric state affected the activity of the class III Fic protein from *Neisseria*
104 *meningitidis* (NmFic) (Stanger *et al*, 2016).

105 Here we report on the biochemical and structural basis of an oligomeric state-dependent
106 switch in FICD's activity, which is well suited to post-translationally regulate protein
107 folding homeostasis in the ER.

108 **Results**

109 **Disrupting the FICD dimer favours BiP AMPylation**

110 Whilst the *FICD* gene is necessary for BiP AMPylation, over-expression of the wild-
111 type FICD enzyme does not result in a detectable pool of BiP-AMP in cells (Preissler
112 *et al*, 2015b). These findings were explained in terms of dominance of the
113 deAMPylation activity of wild-type FICD, as observed in vitro (Preissler *et al*, 2017a).
114 However, somewhere between low-level endogenous expression, which yields
115 physiologically-regulated AMPylation, and over-expression, which precludes BiP-
116 AMP accumulation, retrovirally-rescued *FICD*^{-/-} cells were endowed with a measure of
117 BiP AMPylation (Figure 1A and S1A-C). This finding points to a protein-dosage effect
118 on wild-type FICD's activity and suggests that the enzymatic mode of (recombinant)
119 FICD may be affected by its concentration in the ER.

120 Purified FICD forms a homodimeric complex in vitro (Bunney *et al*, 2014). Co-
121 expression of reciprocally-tagged FICD confirmed that the wild-type protein forms
122 homomeric complexes in cells that are disrupted by a previously characterised
123 Leu258Asp mutation within the major dimerisation surface (Bunney *et al*, 2014)
124 (Figure 1B). Unlike the wild-type dimerisation-competent enzyme, at a similar level of
125 over-expression, the monomeric FICD^{L258D} yielded a clear BiP-AMP signal in *FICD*^{-/-}
126 cells (Figure 1C). This pool was conspicuous even under basal conditions, in which
127 wild-type cells have only a weak BiP-AMP signal, suggesting that the imposed
128 monomeric state deregulated FICD's activity.

129 Together, these observations intimate that dynamic changes in the equilibrium between
130 the monomer and dimer may contribute to a switch between FICD's mutually
131 antagonistic activities – AMPylation and deAMPylation of BiP. Increasing its
132 concentration by over-expression favours FICD dimerisation and thus perturbs such
133 regulatory transitions. This could account for the observation that FICD
134 overexpression, in unstressed wild-type cells, abolishes the small pool of BiP-AMP
135 normally observed under basal conditions (Preissler *et al*, 2017b).

136 Size-exclusion chromatography (SEC) and analytical ultracentrifugation (AUC), with
137 purified proteins, confirmed the stability of the FICD dimer (Figure 1D-E and S1D-G).
138 These techniques also confirmed the strong disrupting effect of the Leu258Asp
139 mutation (in the principal dimer surface) and revealed a weaker disrupting effect of a

140 Gly299Ser mutation (in the secondary dimer surface) (Figure S1D-G). AUC yielded a
141 1.2 nM dimer dissociation constant (K_d) of wild-type FICD and SEC indicated a K_d in
142 the millimolar range for FICD^{L258D} and a K_d of 9.5 μ M for FICD^{G299S}. We therefore
143 conclude that between 0.2 μ M and 5 μ M (concentrations at which the experiments that
144 follow were performed) the wild-type protein is dimeric, FICD^{L258D} is monomeric, and
145 FICD^{G299S} is partially monomeric.

146 In the presence of [α -³²P]-ATP both FICD^{L258D} and FICD^{G299S} established a pool of
147 AMPylated, radioactive BiP in vitro [Figure 1F; also observed in the *Drosophila*
148 counterpart of FICD^{L258D} (Casey *et al*, 2017)], whereas the wild-type enzyme did not,
149 as previously observed (Preissler *et al*, 2015b, 2017a). BiP is a substrate for
150 AMPylation in its monomeric, ATP-bound, domain-docked conformation (Preissler *et*
151 *al*, 2015b, 2017b). These experiments were therefore performed with an ATPase-
152 deficient, oligomerisation-defective, ATP-bound BiP mutant, BiP^{T229A-V461F}. Thus, the
153 BiP-AMP signal is a result of the concentration of substrate (unmodified and modified
154 BiP) and the relative AMPylation and deAMPylation activities of the FICD enzyme.
155 As expected, a strong BiP-AMP signal was elicited by the unrestrained AMPylation-
156 active FICD^{E234G} (which cannot deAMPylate BiP). FICD^{E234G-L258D} gave rise to a
157 similar, but reproducibly slightly weaker, BiP-AMP signal relative to FICD^{E234G}.

158 Monomerisation switches FICD's enzymatic activities

159 The ability of the dimer interface FICD mutants to yield a detectable BiP-AMP signal
160 in vitro agreed with the in vivo data and suggested a substantial change in the regulation
161 of the enzyme's antagonistic activities – either inhibition of deAMPylation, de-
162 repression of AMPylation, or a combination of both. To distinguish between these
163 possibilities, we analysed the deAMPylation activities of the FICD mutants in an assay
164 that uncouples deAMPylation from AMPylation. As previously observed, wild-type
165 FICD caused the release of fluorescently labelled AMP from in vitro AMPylated BiP,
166 whereas FICD^{E234G} did not (Preissler *et al*, 2017a) (Figure 2A). FICD^{L258D} and
167 FICD^{G299S} consistently deAMPylated BiP 2-fold slower than the wild-type (Figure 2A
168 and S2A). The residual in vitro deAMPylation activity of FICD^{L258D} and the absence
169 of such activity in FICD^{E234G} is consistent with the divergent effect of expressing these
170 deregulated mutants on a UPR reporter in cells (Figure S2B-C).

171 The FICD-mediated BiP AMPylation/deAMPylation cycle converts the co-substrate
172 ATP to the end products AMP and pyrophosphate (Preissler *et al.*, 2017a). We exploited
173 this feature to quantify enzymatic activity. FICD was incubated with [α - 32 P]-ATP,
174 either in the presence or absence of ATPase-deficient BiP^{T229A}, and accumulation of
175 radioactive AMP was measured by thin layer chromatography. Only background levels
176 of AMP were generated by catalytically inactive FICD^{H363A} or FICD^{E234G-H363A} (Figure
177 2B). The deregulated, deAMPylation-defective FICD^{E234G} yielded a weak AMP signal
178 that was not increased further by the presence of BiP, suggesting that the Glu234Gly
179 mutation enables some BiP-independent ATP hydrolysis to AMP. Conversely, small
180 but significant amounts of AMP were produced by wild-type FICD but in a strictly BiP-
181 dependent fashion (Figure 2B-C and Figure S2D). These observations are consistent
182 with a slow, FICD-driven progression through the BiP AMPylation/deAMPylation
183 cycle indicating incomplete repression of wild-type FICD's AMPylation activity under
184 these conditions. As expected, abundant BiP-dependent AMP production was observed
185 in reactions containing AMPylation-active FICD^{E234G} alongside deAMPylation-active
186 wild-type FICD (Figure 2B, lane 11). Importantly, large amounts of AMP were also
187 generated when BiP was exposed to FICD^{L258D} and, to lesser extent, FICD^{G299S} (Figure
188 2C and S2D). Together, these observations suggest that the AMPylation activities of
189 the monomeric FICD mutants are significantly enhanced relative to the wild-type,
190 whilst their deAMPylation activities are more modestly impaired.

191 To directly assess the AMPylation activities of bifunctional FICDs we exploited the
192 high affinity of the catalytically inactive FICD^{H363A} for BiP-AMP, as a “trap” that
193 protects BiP-AMP from deAMPylation (Figure 2D). To disfavour interference with the
194 FICD enzyme being assayed we engineered the trap as a covalent disulfide linked dimer
195 incapable of exchanging subunits with the active FICD being assayed. A cysteine
196 (Ala252Cys) was introduced into the major dimerisation surface of the trap. To
197 preclude aberrant disulphide bond formation, the single endogenous cysteine of FICD
198 was also replaced (Cys421Ser). After purification and oxidation, this protein (s -
199 s FICD^{A252C-H363A-C421S}; the trap) formed a stable disulphide-bonded dimer (Figure S2E-
200 F) that tightly bound BiP-AMP with fast association and slow dissociation kinetics
201 (Figure S2G-H). Moreover, the binding of the trap to unmodified BiP was, in
202 comparison, negligible (Figure S2G). We reasoned that adding the trap in excess to
203 reactions assembled with BiP, ATP and FICD would sequester the BiP-AMP product

204 and prevent its deAMPylation, enabling the comparison of AMPylation rates in
205 isolation from the deAMPylating activity.

206 In presence of the trap, wild-type FICD produced a detectable BiP-AMP signal; but not
207 in the absence of the trap (compare [Figures 1F](#) and [2E](#)). Importantly, presence of the
208 trap revealed that AMPylation of BiP was greatly accelerated by FICD monomerisation
209 (> 19-fold compared to the wild-type) ([Figure 2E](#)). As expected, BiP AMPylation by
210 FICD^{E234G} was even faster.

211 If the enhanced AMPylation activity of the dimerisation-defective mutants, observed
212 above, truly represents divergent enzymatic activities of different FICD oligomeric
213 states, it should be possible to reveal this feature by diluting the wild-type enzyme to
214 concentrations at which an appreciable pool of monomer emerges. In AMPylation
215 reactions set up with [α -³²P]-ATP a detectable signal from radiolabelled BiP-AMP was
216 noted at enzyme concentrations near the K_d of dimerisation (between 10 and 2.5 nM;
217 [Figure 3A, left](#)). The inverse relationship of enzyme concentration to the BiP-AMP
218 signal likely reflects the opposing activities and relative populations of AMPylation-
219 biased FICD monomers and the deAMPylation-biased FICD dimers in each reaction.
220 This counter-intuitive relationship of enzyme to product is resolved in the presence of
221 the AMPylation trap; the BiP-AMP signal increased in a time- and enzyme
222 concentration-dependent manner, as expected from a reaction which is proportional to
223 the absolute concentration of monomeric enzyme ([Figure 3A, right](#)). In the presence of
224 the trap the shift in the peak of the BiP-AMP signal, after 16 hours, towards lower
225 concentrations of FICD, likely reflects incomplete protection of AMPylated BiP by the
226 trap and its enhanced susceptibility to deAMPylation at higher concentrations of
227 (dimeric) FICD.

228 If monomerisation significantly enhances AMPylation activity, constitutive FICD
229 dimers that are unable to dissociate should have low AMPylation activity and fail to
230 produce modified BiP even under dilute conditions. To test this prediction, we created
231 a disulphide-linked wild-type FICD (s -sFICD^{A252C-C421S}), which, after purification and
232 oxidation, formed a covalent dimer ([Figure S3A](#)). Moreover, its SEC profile was
233 indistinguishable from wild-type FICD or the cysteine-free counterpart, FICD^{C421S}
234 ([Figure S3B](#)). In the presence of the BiP-AMP trap, oxidised s -sFICD^{A252C-C421S}
235 produced significantly less AMPylated BiP than either wild-type or FICD^{C421S} at
236 similar concentrations ([Figure 3B, lane 8](#) and [S3C](#)).

237 Repression of AMPylation was imposed specifically by the covalent dimer, as non-
238 oxidised FICD^{A252C-C421S} elicited a conspicuous pool of BiP-AMP - more than the wild-
239 type enzyme (Figure 3B, lane 9 and S3C) - an observation explained by the weakening
240 of the FICD dimer imposed by the Ala252Cys mutation (Figure S1D-E). Similarly, in
241 absence of the trap, the ability of pre-oxidised s-sFICD^{A252C-C421S} to establish a pool of
242 AMPylated BiP was greatly enhanced by diluting the enzyme into a buffer containing
243 DTT. FICD^{C421S}, by contrast, produced similar amounts of modified BiP under both
244 non-reducing and reducing conditions (Figure 3C).

245 DeAMPylation activities of oxidised and non-oxidised FICD^{A252C-C421S} were
246 comparable and similar to wild-type FICD (Figure 3D-E, S2A and S3D), pointing to
247 the integrity of these mutant enzymes. Together, these observations argue that covalent
248 s-sFICD^{A252C-C421S} dimers selectively report on the enzymatic characteristics of wild-
249 type FICD in its dimeric state. This protein therefore serves to help validate the
250 conclusion that a low concentration of wild-type FICD favours the formation of
251 monomers, whose AMPylation activity is de-repressed, to promote BiP modification.

252 **An AMPylation-repressive signal is transmitted from the dimer interface to the** 253 **active site**

254 The crystal structure of dimeric FICD suggests the existence of a hydrogen-bond
255 network, involving the side-chains of Lys256 and Glu242, linking the dimer interface
256 with the enzyme's active site, impinging on the AMPylation-inhibiting Glu234 (Figure
257 4A). To test this notion, we mutated both putative dimer relay residues. FICD^{K256S} and
258 FICD^{E242A} formed stable dimers, as assayed by SEC, with dimer K_d values under 400
259 nM (Figure 4B and S1D-E). In vitro both mutants established a pool of modified BiP
260 (Figure 4C and S4A). This remained the case even at FICD concentrations in which
261 negligible amounts of monomer are predicted (2 and 10 μ M; Figure S4A). De-
262 repression of AMPylation by these dimer relay mutations was also evidenced by the
263 enhanced BiP-dependent AMP production, relative to wild-type FICD (Figure 4D),
264 whilst deAMPylation activities were similar (Figure S2A and S4B). Combining the
265 Lys256Ser and the monomerising Leu258Asp mutations (FICD^{K256S-L258D}) further
266 enhanced the BiP-AMP pool produced in vitro (Figure S4A), an observation only
267 partially attributable to the concomitant decrease in the deAMPylation rate (Figure S2A
268 and S4C). These observations suggest that residues connecting the dimer interface and

269 the active site contribute to repression of AMPylation and that mutating these residues
270 uncouples a gain-of-AMPylation activity from the oligomeric state of FICD.

271 Transmission of a repressive signal via a network of intramolecular interactions is also
272 supported by the correlation between de-repression of BiP AMPylation and the
273 negative effect of various mutants on the global stability of FICD. Differential scanning
274 fluorimetry (DSF) revealed an inverse relationship between the AMPylation activity
275 and the melting temperature (T_m) of FICD mutants (Figure 4E and S4D). These
276 differences in flexibility were observed despite the fact that the DSF assays were
277 conducted at relatively high protein concentrations (2 μ M) that would favour
278 dimerisation of all but the most dimerisation-defective mutants.

279 Nucleotide binding stabilises all FICD variants (Figure S4D), a feature that is
280 conspicuous in case of the AMPylation de-repressed FICD^{E234G} (Bunney *et al*, 2014).
281 However, monomerisation imposed by the Leu258Asp mutation, did not significantly
282 increase ATP-induced stabilisation of FICD (ΔT_m) (Figure 4F and S4E). Interestingly,
283 although AMPylation activity correlated with increased FICD flexibility this was not
284 reflected in an appreciably altered propensity to bind ATP. This suggested that the
285 variation in enzyme activity of different FICD mutants may arise not from variation in
286 their affinity for nucleotide but from their particular mode of ATP binding. To explore
287 this possibility, we set out to co-crystallise FICD variants with MgATP.

288 **Monomerisation favours AMPylation-competent binding of MgATP**

289 High-resolution X-ray crystal structures of monomeric and dimeric FICD were
290 obtained in various nucleotide bound states (Table 1). The tertiary structure of the Fic
291 domain of both the monomeric FICD^{L258D} and the dimeric relay mutant FICD^{K256S}
292 deviated little from that of the nucleotide-free wild-type dimer structure (FICD:Apo;
293 PDB: 4u04) (Figure 5A and S5A). Moreover, co-crystallisation of FICD^{L258D},
294 FICD^{K256A} or the wild-type dimer with ATP or an ATP analogue (AMPPNP) also
295 resulted in no significant Fic domain conformational change from FICD:Apo (Figure
296 5A and S5A). Accordingly, the greatest root-mean squared deviation (RMSD) between
297 the Fic domain of the FICD:ATP structure and any other monomeric or dimer relay
298 FICD structure is 0.53 Å (observed between FICD:ATP and FICD^{L258D}:Apo; residues
299 213-407). The only conspicuous change in global tertiary structure occurred in the TPR
300 domain of FICD^{L258D} co-crystallised with ATP or AMPPNP, in which the TPR domain

301 is flipped almost 180° from its position in other FICD structures (Figure 5A). Notably,
302 in all FICD structures the α_{inh} remains firmly juxtaposed to the core Fic domain.

303 When co-crystallised with MgATP or MgAMPPNP the resulting FICD structures
304 contained clear densities for nucleotide (Figure 5B and S5B). The AMPylation-biased
305 FICD mutants also contained discernible, octahedrally coordinated Mg²⁺ ions (Figure
306 5Bii-iii and S5B). As noted in other Fic AMPylases, this Mg²⁺ was coordinated by the
307 α - and β -phosphates of ATP/AMPPNP and Asp367 of the Fic motif (Xiao *et al*, 2010;
308 Khater & Mohanty, 2015b; Bunney *et al*, 2014). Interestingly, in the dimeric wild-type
309 FICD:ATP structure, crystallised in the presence of MgATP, there was no density that
310 could be attributed to Mg²⁺ (Figure 5Bi). The only possible candidate for Mg²⁺ in this
311 structure was a water density, located between all three phosphates, that fell in the Fic
312 motif's anion-hole – a position incompatible with Mg²⁺ coordination (Zheng *et al*,
313 2017).

314 Alignment of the nucleotide-bound structures revealed that ATP or AMPPNP were
315 bound very differently by the wild-type dimer and the AMPylation-biased monomeric
316 or dimer relay FICD mutants (Figure 5C and S5C). Concordantly, the RMSD of ATP
317 between the wild-type FICD and monomeric FICD^{L258D} was 2.17 Å (and 2.23 Å for
318 FICD^{K256A}'s ATP). As previously observed in other ATP-bound Fic proteins that
319 possess an inhibitory glutamate, the nucleotide in FICD:ATP was in an AMPylation
320 non-competent conformation (Engel *et al*, 2012; Goepfert *et al*, 2013) that is unable to
321 coordinate Mg²⁺; an essential ion for FICD-mediated AMPylation (Ham *et al*, 2014).
322 Moreover, the position of the ATP α -phosphate precludes in-line nucleophilic attack
323 (by the hydroxyl group of BiP's Thr518) due to the proximity of the flap residue Val316
324 (Figure 5C and S5D). Furthermore, an attacking nucleophile in-line with P α -O3 α
325 would be at a considerable distance from the catalytic His363 (required to deprotonate
326 Thr518's hydroxyl group) (Figure 5Bi, 5C and S5D).

327 By contrast, in the active sites of FICD^{K256A} or FICD^{L258D} MgATP and MgAMPPNP
328 assumed AMPylation-competent conformations: their α -phosphates were in the
329 canonical position (Figure S5E), as defined by AMPylation-active Fic proteins lacking
330 inhibitory glutamates (Xiao *et al*, 2010; Engel *et al*, 2012; Goepfert *et al*, 2013; Bunney
331 *et al*, 2014). As a result, in-line nucleophilic attack into the α - β -phosphoanhydride bond

332 of ATP would not be sterically hindered and the Nε2 of His363 would be well
333 positioned for general base catalysis (Figure 5C and S5C-D).

334 The presence of ATP in both dimeric wild-type FICD and monomeric FICD^{L258D}
335 (although in different binding modes) is consonant with the DSF data (Figure 4F and
336 S4E). Apart from Glu234, the residues directly interacting with ATP are similarly
337 positioned in all structures (maximum RMSD 0.83 Å). However, considerable
338 variability is observed in Glu234, with an RMSD of 4.20 Å between monomeric and
339 dimeric wild-type ATP structures, which may hint at the basis of monomerisation-
340 induced AMPylation competency. In ATP-bound structures the inhibitory glutamate is
341 displaced from the respective apo ground-state position, in which it forms an inhibitory
342 salt-bridge with Arg374: R₂ of the Fic motif (Figure S6A). However, the displacement
343 of the Glu234 side chain observed in the FICD:ATP structure (from its position in
344 FICD:Apo; PDB 4u0u) would be insufficient for AMPylation-competent binding of the
345 γ-phosphate of an ATP/AMPPNP (see distances i and ii, Figure 5C and S5C). This
346 steric clash is relieved by the side chain conformations observed in the AMPylation-
347 competent structures (see iii and iv, Figure 5C and S5C).

348 The findings above suggest that the AMPylation-biased FICD mutants attain their
349 ability to competently bind MgATP by increased flexibility at the top of the α_{inh} and by
350 extension through increased Glu234 dynamism. It is notable that all the nucleotide
351 triphosphate-bound FICDs crystallised with intact dimer interfaces (Figure S6A and
352 B). Moreover, with the exception of direct hydrogen bonds to mutated Lys256 side
353 chains, in all FICD crystals the putative dimer relay hydrogen-bond network was
354 maintained (Figure S6A). It seems likely that much of the monomerisation-linked
355 conformational flexibility that facilitates binding of MgATP in solution cannot be
356 trapped crystallographically. Nonetheless, comparing B-factors across the nucleotide
357 triphosphate-bound FICD structures is informative: despite similar crystal packing
358 (Figure S6B) the average residue B-factors, both in the dimerisation interface and near
359 Glu234, positively correlated with the AMPylation activities of the respective mutants
360 (Figure S7).

361 **ATP is an allosteric modulator of FICD**

362 Given the conspicuous difference in the ATP binding modes observed between
363 AMPylation-competent FICD mutants and the AMPylation-incompetent wild-type

364 dimeric FICD, we were intrigued by the possibility that ATP may modulate other
365 aspects of FICD enzymology and regulation.

366 In order to explore the effects of nucleotide on the different pre-AMPylation complexes
367 formed between either dimeric or monomeric FICD and its co-substrate, ATP-bound
368 BiP, we utilised BioLayer Interferometry (BLI). Biotinylated, client-binding-impaired,
369 ATPase-defective BiP^{T229A-V461F} was made nucleotide free (Apo) and immobilised on
370 a streptavidin biosensor. Its interactions with catalytically inactive, dimeric FICD^{H363A}
371 or catalytically inactive, monomeric FICD^{L258D-H363A} were measured in the presence
372 and absence of nucleotides. The binding of both monomeric and dimeric FICD to
373 immobilised BiP was greatly enhanced by the pre-saturation of BiP with ATP (Figure
374 6A and S8A). This is consistent with ATP-bound BiP as the substrate for FICD-
375 mediated AMPylation (Preissler *et al*, 2015b). Moreover, the binding signal produced
376 by immobilised, ATP-bound BiP interacting with monomeric FICD^{L258D-H363A}:Apo was
377 significantly stronger than that produced from the corresponding dimeric
378 FICD^{H363A}:Apo analyte (Figure 6A). In contrast, AMPylated BiP bound more tightly to
379 dimeric FICD^{H363A} than to monomeric FICD^{L258D-H363A} (forming a pre-deAMPylation
380 complex, Figure S2G). These findings align with the role of dimeric FICD in
381 deAMPylation and the monomer in AMPylation.

382 Interestingly, in presence of magnesium bound nucleotide (either MgATP or MgADP)
383 the FICD^{H363A} interaction with ATP-bound BiP was weakened (Figure 6A). This effect
384 was considerably more pronounced for monomeric FICD^{L258D-H363A}. To quantify the
385 effect of FICD monomerisation on the kinetics of pre-AMPylation complex
386 dissociation, BLI probes preassembled with biotinylated, ATP-bound BiP and either
387 apo dimeric FICD^{H363A} or apo monomeric FICD^{L258D-H363A} were transferred into
388 otherwise identical solutions \pm ATP (schematised in Figure S8B). The ensuing
389 dissociations fit biphasic exponential decays and revealed that ATP binding to FICD
390 accelerated the dissociation of monomeric FICD^{H363A} more than dimeric FICD^{H363A}
391 (Figure 6B and S8C). The effect of ATP was noted on both the slow dissociation phase
392 of the monomer ($k_{\text{off,slow}}$; Figure 6C-D) and on the percentage of dissociation attributed
393 to the fast phase (%Fast; Figure 6D and S8D). The effect of ATP on the dissociation
394 kinetics of the FICD^{L258D-H363A}/BiP:ATP complex, measured under conditions of
395 effectively infinite dilution, argues against a simple one-site competition between ATP-

396 bound BiP and ATP for the Fic domain active site. Instead, these observations are better
397 explained as allosteric modulation of monomeric FICD by ATP.

398 The structural data indicates that FICD's oligomeric state can impact significantly on
399 the mode of ATP binding, and [Figure 6B](#) indicates an allosteric effect of nucleotide
400 binding on FICD. Together these observations suggested bi-directional intramolecular
401 signalling from the dimer interface to the nucleotide-binding active site and therefore
402 the possibility that ATP binding in FICD's active site may also influence the oligomeric
403 state of the protein. To investigate this hypothesis, hetero-dimers of N-terminally
404 biotinylated FICD^{H363A} assembled with non-biotinylated FICD^{H363A} were loaded onto
405 a BLI streptavidin biosensor. The dissociation of non-biotinylated FICD^{H363A} from its
406 immobilised partner was then observed by infinite dilution into buffers varying in their
407 nucleotide composition ([Figure 6E](#) and [S8E](#), schematised in [Figure 6F](#)). ATP but not
408 ADP induced a 3-fold increase in the dimer off rate ([Figure 6G](#)). This is suggestive of
409 a mechanism whereby changing ATP/ADP ratios in the ER may modulate the
410 oligomeric state of FICD.

411

412 Discussion

413 This study addresses a key process in the post-translational UPR by which bifunctional
414 FICD switches between catalysis of BiP AMPylation and deAMPylation, in order to
415 match the folding capacity of the ER to the burden of unfolded proteins independently
416 of changes in gene expression. The high affinity of FICD protomers for each other
417 specifies the presence of principally dimeric FICD in the ER, shown here to restrict the
418 enzyme to deAMPylation. This is the dominant mode of FICD both in vitro and in cells
419 under basal conditions (Preissler *et al*, 2017a; Casey *et al*, 2017). However, establishing
420 a pool of monomeric FICD unmask its potential as a BiP AMPylase and enfeebles
421 deAMPylation. The structural counterpart to this switch is the mode by which MgATP,
422 the AMPylation reaction's co-substrate, is productively engaged in the active site of the
423 monomeric enzyme. Our studies suggest that monomerisation relieves the repression
424 imposed on FICD AMPylation by weakening a network of intramolecular contacts. In
425 the repressed state these contacts propagate from the dimer interface to the enzyme's
426 active site and stabilise a conserved inhibitory residue, Glu234, to block AMPylation-
427 competent binding of MgATP (Figure 7).

428 Our observations of a biphasic FICD concentration-dependent rescue of BiP
429 AMPylation in *FICD*^{-/-} cells and the conspicuous ability of the monomerising
430 Leu258Asp mutation to establish a modified BiP pool in *FICD*^{-/-} cells, all support an
431 oligomeric state-dependent switch as a key contributor to FICD regulation in vivo. This
432 case is further supported by the divergent enzymatic properties of monomeric mutants
433 and enforced disulphide-linked dimers in vitro, and by measurements of the enzymatic
434 activity of wild-type FICD in concentration regimes above and close to the dimerisation
435 K_d . Complete monomerisation resulted in a 19-fold increase in AMPylation activity and
436 a 2-fold decrease in deAMPylation activity. The concordance between monomeric
437 FICD^{L258D}, dimerisation-defective mutants, and mutants in the repressive relay from
438 the dimer interface to the active site gives confidence in the validity of the biophysical
439 and structural insights provided by the mutants.

440 The inverse correlation observed between the thermal stability of FICD mutants and
441 their AMPylation activity, supports a role for enhanced flexibility in enabling the
442 enzyme to attain the conformation needed for catalysis of this reaction – a role clarified
443 by the crystallographic findings (see below). The biophysical assays also suggest that
444 monomeric FICD is more allosterically sensitive to ATP binding, as it exhibits a

445 pronounced nucleotide-dependent reduction in the affinity for its co-substrate, ATP-
446 bound BiP. The observation that ATP significantly accelerated the dissociation of
447 monomeric, nucleotide-free FICD from ATP-bound BiP suggests that this feature of
448 the monomer is mediated allosterically (not by enhanced susceptibility of a destabilised
449 protein to co-substrate competition for the same active site). The lower affinity of
450 monomeric FICD for its BiP:ATP co-substrate, in the context of a quaternary pre-
451 AMPylation complex, conspicuously distinguishes it from the dimer and is a feature
452 that may also enhance AMPylation rates: ground-state destabilisation has been
453 demonstrated in a number of enzymes as a means of catalytic rate enhancement, by
454 reducing the otherwise anti-catalytic tight binding of an enzyme to its substrate
455 (Andrews *et al*, 2013; Ruben *et al*, 2013).

456 A structure of the quaternary pre-AMPylation complex, that could inform our
457 understanding of the features of the monomeric enzyme, does not exist. Nevertheless,
458 important insights into the effect of monomerisation were provided by structures of
459 FICD and its nucleotide co-substrate. Dimeric wild-type FICD binds ATP (without
460 magnesium) in an AMPylation incompetent mode. This is consistent with all other
461 inhibitory glutamate containing Fic structures crystallised with ATP or ATP analogues
462 (Engel *et al*, 2012; Goepfert *et al*, 2013). In stark contrast, we have discovered that
463 despite the presence of an inhibitory glutamate, monomerisation, or mutations in
464 residues linking the dimer interface to Glu234, permit the binding of ATP with
465 magnesium in a conformation competent for AMPylation.

466 Our studies suggest that the disparity in FICD's ATP binding modes stems from a
467 monomerisation-induced increase in Glu234 flexibility (mediated by weakening of the
468 dimer relay). This increase in flexibility is reflected in relatively subtle changes in the
469 Glu234 side chain position, B-factor increases in the respective crystal structures, and
470 markedly lower melting temperature of FICD^{K256A} and FICD^{L258D} relative to the wild-
471 type dimer.

472 It seems likely that in solution monomerisation allows greater flexibility in this dimer
473 relay network, facilitating motion and possibly unfolding at the top of the Glu234
474 containing α -helix (α_{inh}). Such considerations could explain the comparatively small
475 differences in the position of Glu234, but stark differences in nucleotide conformation,
476 observed between the dimeric wild-type and monomeric or dimer relay mutant

477 structures. That is to say, in solution the mutants exhibit sufficiently increased Glu234
478 dynamics to permit binding of MgATP in a catalytically competent mode. However,
479 the crystallisation process quite possibly favours rearrangements, including α_{inh}
480 refolding and crystallographic reconstitution of the dimer interface, and convergence
481 towards a low energy state (the one stabilised in solution by dimerisation). This then
482 outweighs the energetic penalty of the resulting (crystallographically-induced)
483 electronically or sterically strained carboxylate-carboxylate (Glu234-Glu263) or
484 glutamate-phosphate contacts (Figure 5C and S5C). Crystallisation may therefore
485 facilitate the apparent convergence of mutant FICD Glu234 conformations towards that
486 imposed in solution by the dimer. By contrast, dimeric wild-type FICD is never able to
487 bind MgATP competently, either in solution or in crystallo, due to its unperturbed
488 allosteric dimer relay and consequently inflexible Glu234.

489 Oligomerisation state-mediated regulation of AMPylation is not unique to FICD.
490 Tetramerisation of bacterial NmFic antagonises auto-AMPylation and AMPylation of
491 its substrate, DNA gyrase (Stanger *et al*, 2016). Though the surfaces involved in
492 oligomerisation of this class III Fic protein are different from that of FICD, these two
493 repressive mechanisms converge on the state of their α_{inhS} . As such, divergent Fic
494 proteins potentially exploit, for regulatory purposes, an intrinsic metastability of this
495 structurally conserved inhibitory α -helix (Garcia-Pino *et al*, 2008). Interestingly, the
496 more extensive dimerisation surface of FICD (which contains Leu258 and is situated
497 at the boundary of the Fic domain core and the N-terminal Fic domain extension) also
498 acts as a structurally conserved dimer interface in other class II bacterial Fic proteins:
499 CdFic (Dedic *et al*, 2016) and *Bacteroides thetaiotaomicron* (BtFic; PDB: 3cuc), but
500 not in the monomeric *Shewanella oneidensis* Fic (SoFic) protein (Goepfert *et al*, 2013).
501 Moreover, a His57Ala mutation in dimeric CdFic (which is structurally equivalent to
502 FICD^{K256A}) causes increased solvent accessibility and auto-AMPylation of a region
503 homologous to the loop linking FICD's Glu242-helix and the α_{inh} (Dedic *et al*, 2016).
504 Despite differences in detail, these findings suggest the conservation of a repressive
505 relay from the dimer interface to the active site of dimeric Fic proteins.

506 Our biophysical observations also suggest a reciprocal allosteric signal propagated
507 from FICD's nucleotide binding site back to the dimer interface; enhanced dimer
508 dissociation was induced by ATP but not ADP. Consequently, it is tempting to

509 speculate that FICD's oligomeric state and hence enzymatic activity might be regulated
510 by the ADP/ATP ratio in the ER. Under basal conditions, low ADP concentrations
511 allow ATP to bind both the monomeric and dimeric pools of FICD, shifting the
512 equilibrium towards the monomer and favouring BiP AMPylation. Stress conditions
513 may increase ADP concentration in the ER (perhaps by increased ER chaperone
514 ATPase activity). This increase would be proportionally much greater than the
515 concomitant decrease in [ATP] (in terms of respective fold changes in concentration).
516 The increased [ADP] would therefore be able to effectively compete with ATP for the
517 monomer-dimer FICD pools and thereby shift the equilibrium back towards the BiP de-
518 AMPylating FICD dimer.

519 The regulation of BiP by FICD-mediated AMPylation and deAMPylation provides the
520 UPR with a rapid post-translational strand for matching the activity of a key ER
521 chaperone to its client load. The simple biochemical mechanism proposed here for the
522 requisite switch in FICD's antagonistic activities parallels the regulation of the UPR
523 transducers, PERK and IRE1, whose catalytically-active conformation is strictly linked
524 to dimerisation (Dey *et al*, 2007; Lee *et al*, 2008). A simple correlation emerges,
525 whereby ER stress favours dimerisation of UPR effectors, activating PERK and IRE1
526 to regulate gene expression and the FICD deAMPylyase to recruit BiP into the chaperone
527 cycle (possibly through an increased ER ADP/ATP ratio). Resolution of ER stress
528 favours the inactive monomeric state of PERK and IRE1 and, as suggested here, the
529 AMPylation-competent monomeric FICD ([Figure 7](#)).

530

531 **Accession Numbers**

532 The FICD crystal structures have been deposited in the PDB with the following
533 accession codes: 6i7g (FICD:ATP), 6i7h (FICD^{K256S}:Apo), 6i7i (FICD^{K256A}:MgATP),
534 6i7j (FICD^{L258D}:Apo), 6i7k (FICD^{L258D}:MgATP), and 6i7l (FICD^{L258D}:MgAMP-PNP).

535

536 **Acknowledgements**

537 We thank the Huntington lab for access to the Octet machine, Claudia Flandoli for
538 scientific illustrations and the CIMR flow cytometry core facility team (Reiner Schulte,
539 Chiara Cossetti and Gabriela Grondys-Kotarba). This work was supported by
540 Wellcome Trust Principal Research Fellowship to D.R. (Wellcome
541 200848/Z/16/Z), Medical Research Council PhD programme funding to L.A.P.
542 (MR/K50127X/1), a Wellcome Trust Principal Research Fellowship to R.J.R.
543 (Wellcome 082961/Z/07/Z), and a Wellcome Trust Strategic Award to the Cambridge
544 Institute for Medical Research (Wellcome 100140).

545

546 **Author contributions**

547 L.A.P. co-led and conceived the project, designed and conducted the biophysical
548 experiments, analysed and interpreted the data, purified and crystallised proteins,
549 collected, analysed and interpreted the X-ray diffraction data, and wrote the manuscript.
550 C.R. designed, conducted and interpreted the in vivo experiments and contributed to
551 revising the manuscript. Y.Y. supervised crystallisation efforts as well as the collection
552 and processing of the X-ray diffraction data, contributed to analysis and interpretation
553 of the structural data and to revising the manuscript. L.N. contributed to the in vivo
554 experiments. S.H.M. conducted the AUC experiments and analysed the AUC data, and
555 contributed to revising the manuscript. R.J.R. contributed to analysis and interpretation
556 of the structural data and to revising the manuscript. D.R. conceived and oversaw the
557 project, interpreted the data, and wrote the manuscript. S.P. co-led and conceived the
558 project, designed and conducted the biochemical experiments, analysed and interpreted
559 the data, and wrote the manuscript.

560

561

562 **Declaration of interests**

563 We declare no conflicts of interests.

564

565 **Figure legends**

566 **Figure 1**

567 **Monomeric mutant FICD promotes BiP AMPylation**

568 **A)** Immunoblot of endogenous BiP resolved by native-PAGE from lysates of CHO-K1
569 S21 wild-type (wt) or *FICD*^{-/-} cells either transiently overexpressing wild-type FICD
570 (high expression level; Hi) or mutant FICD^{E234G} (E/G) or stably expressing recombinant
571 wild-type FICD (low expression level; Lo). The cells in lanes 1-4 were mock
572 transfected. Where indicated cells were exposed to cycloheximide (CHX; 100 µg/mL)
573 for 3 h before lysis. Unmodified ('A') and AMPylated ('B') monomeric and oligomeric
574 (II and III) forms of BiP are indicated. Immunoblots of the same samples resolved by
575 SDS-PAGE report on FICD, total BiP and eIF2α (loading control). Data representative
576 of four independent experiments are shown. See [Figure S1B-C](#).

577 **B)** Wild-type FICD forms homomeric complexes in vivo. Immunoblots of
578 orthogonally-tagged wild-type and Leu258Asp mutant FICD in the input cell lysate and
579 following recovery by pull-down with streptavidin (recognizing the AviTag) or anti-
580 FLAG antibody. Proteins were detected with fluorescently-labelled streptavidin
581 (StrepIR800) or FLAG antibody. Data representative of three independent experiments
582 are shown.

583 **C)** Immunoblot of endogenous BiP from transfected CHO-K1 S21 *FICD*^{-/-} cells (as in
584 A). Note that cells expressing monomeric FICD^{L258D} accumulate AMPylated BiP. Data
585 representative of three independent experiments are shown.

586 **D)** Size-exclusion chromatography (SEC) analysis of wild-type and mutant FICD
587 proteins (each at 20 µM). The elution times of protein standards are indicated as a
588 reference. Note that the Leu258Asp mutation monomerises FICD, while Gly299Ser
589 causes partial monomerisation. See [Figure S1D-E](#).

590 **E)** Comparison of the signal-averaged sedimentation coefficients of wild-type (red) and
591 monomeric mutant FICD^{L258D} (blue), as measured by analytical ultracentrifugation. A
592 fit for monomer-dimer association (solid red line), constrained using the average value
593 for the monomeric protein (dashed line, 2.82 S, $S_{w,20} = 3.02$ S), yielded a K_d of 1.2 nM
594 with a 95% confidence interval between 1.1 to 1.4 nM and a value of 4.08 S for the
595 dimer ($S_{w,20} = 4.36$ S). The fitted data points are from three independent experiments.
596 See [Figure S1F-G](#).

597 **F)** Autoradiograph of BiP, AMPylated in vitro by the indicated FICD derivatives, with
598 [α -³²P]-ATP as a substrate and resolved by SDS-PAGE. Proteins in the gel were
599 visualized by Coomassie staining. A representative result of three independent
600 experiments is shown.

601

602

603 **Figure 2**

604 **Monomerising mutations de-repress FICD's AMPylation activity**

605 **A)** Monomerising FICD mutations inhibit deAMPylation. Shown is a representative
606 plot of data points and fit curves of the time-dependent deAMPylation of a fluorescent
607 BiP^{V461F}-AMP^{FAM} by the indicated FICD proteins (at 7.5 μ M) as detected by a change
608 in fluorescence polarisation (FP). DeAMPylation rates calculated from independent
609 experiments are given in [Figure S2A](#).

610 **B-C)** Dimer interface mutants both AMPylate and deAMPylate BiP. Shown are
611 representative autoradiographs of thin layer chromatography (TLC) plates revealing
612 AMP produced from reactions containing [α -³²P]-ATP and the indicated FICD
613 enzymes in the presence or absence of the co-substrate BiP (arrow indicates direction
614 of nucleotide migration). The radioactive signals were quantified and the AMP signals
615 were normalised to the total nucleotide signal in each sample. Plotted below are mean
616 values \pm SD from at least three independent experiments. Unpaired t-tests were
617 performed. See [Figure S2D](#).

618 **D)** Cartoon depicting sequestration of AMPylated BiP by a covalently linked,
619 disulphide-stapled, s-sFICD^{A252C-H363A-C421S} dimer (trap). See [Figure S2E-H](#).

620 **E)** Detection of the time-dependent accumulation of AMPylated BiP^{T229A-V461F} in
621 radioactive reactions, containing [α -³²P]-ATP and the indicated FICD proteins, in the
622 presence of excess trap. At the specified time-points samples were taken and analysed
623 by SDS-PAGE. The autoradiograph (³²P) illustrates the radioactive signals, which
624 represent AMPylated BiP; proteins were visualized by Coomassie staining. The
625 radioactive signals were quantified and presented in the graph below. Mean values \pm
626 SD of three independent experiments are shown.

627

628 **Figure 3**

629 **Monomerisation by dilution enhances the AMPylation activity of wild-type FICD**

630 **A)** Autoradiographs of in vitro reactions containing varying concentration of wild-type
631 FICD protein and fixed concentrations of BiP^{T229A-V461F} and [α -³²P]-ATP as co-
632 substrates, resolved by SDS-PAGE after the indicated incubation times. The proteins
633 were visualized by Coomassie staining of the gel (bottom). The reactions shown on the
634 right were performed in the presence of an excess of s-sFICD^{A252C-H363A-C421S} (trap) to
635 delay de-modification of BiP. Representative gels are shown, and similar results were
636 observed in three independent experiments.

637 **B)** As in (A) but with 0.2 μ M of the indicated FICD variant. The radioactive signals
638 were detected by autoradiography, quantified, and normalised to the signal in lane 6.
639 The mean radioactive signals \pm SD from three independent experiments are given. The
640 proteins were visualized by staining with Coomassie. See [Figure S3A-B](#).

641 **C)** As in (A) but with dilutions of FICD^{C421S} or covalently linked s-sFICD^{A252C-C421S}.
642 Reactions were preceded by a 16 h incubation of FICD in presence or absence of the
643 reducing agent (DTT). Representative gels are shown of three independent
644 experiments. See [Figure S3C](#).

645 **D)** Forced dimerisation does not significantly alter deAMPylation rates. Time-
646 dependent deAMPylation of fluorescent BiP^{V461F}-AMP^{FAM} by the indicated FICD
647 proteins (at 7.5 μ M) assayed by fluorescence polarisation (as in [Figure 2A](#)). A
648 representative experiment (data points and fit curves) is shown and rates are given in
649 [Figure S2A](#). See [Figure S3D](#).

650 **E)** Representative autoradiograph of thin layer chromatography (TLC) plates revealing
651 AMP produced from reactions containing [α -³²P]-ATP and the indicated FICD
652 enzymes in the presence of the co-substrate BiP. AMP signals were normalised to the
653 total nucleotide signal in each sample and the graph below plots mean values \pm SD from
654 at least three independent experiments.

655

656 **Figure 4**

657 **Residues connecting the FICD dimer interface with the inhibitory α -helix stabilise**
658 **FICD and repress AMPylation**

659 **A)** Ribbon diagram of the FICD dimer interface with monomers in purple and blue
660 ribbons (PDB:6i7g). Residues involved in a H-bond network linking the dimer interface
661 to the α_{inh} (as well as Gly299 and Glu234) are shown as green sticks. Sub-3.50 Å
662 hydrogen bonds made by Asn236, Leu238 and Lys256 are depicted as dotted cyan
663 lines.

664 **B)** Size-exclusion chromatography elution profile of wild-type and mutant FICD
665 proteins (each at 20 μ M). Protein absorbance at 280 nm is plotted against elution time.
666 The elution times of protein standards are indicated as a reference.

667 **C)** Radioactive in vitro AMPylation reactions containing the indicated FICD proteins,
668 [α -³²P]-ATP, and BiP^{T229A-V461F} were analysed by SDS-PAGE. The radioactive BiP-
669 AMP signals were detected by autoradiography and proteins were visualized by
670 Coomassie staining of the gel. See [Figure S4A](#).

671 **D)** Representative autoradiograph of thin layer chromatography (TLC) plates revealing
672 AMP produced from reactions containing [α -³²P]-ATP and the indicated FICD
673 enzymes in the presence of the co-substrate BiP. The radioactive signals were
674 quantified and the AMP signals were normalised to the total nucleotide signal in each
675 sample. The graph shows mean AMP values \pm SD from three independent experiments.

676 **E)** Melting temperatures (T_m) of the indicated FICD mutants (at 2 μ M) were measured
677 by differential scanning fluorimetry (DSF). Shown is the mean $T_m \pm$ SD of three
678 independent experiments. The inset shows melt curves with their negative first
679 derivatives from a representative experiment. See [Figure S4D](#).

680 **F)** A plot of the melting temperature of the indicated FICD proteins in absence (Apo)
681 or presence of nucleotides. Shown are the mean T_m values \pm SD of three independent
682 DSF experiments. Monomeric FICD^{L258D} (mFICD) and FICD^{L258D-E234G} (mFICD^{E/G})
683 as well as dimeric wild-type FICD (dFICD) and FICD^{E234G} (dFICD^{E/G}) were tested.
684 ADP and ATP concentrations in mM are given in parentheses. See [Figure S4E](#) for $K_{1/2}$
685 quantification.

686 **Figure 5**

687 **Monomeric FICD binds ATP in an AMPylation-competent conformation**

688 **A)** Monomerisation does not result in large conformational changes in FICD. Shown is
689 the alignment, from residues 213-407, of FICD molecules in the asymmetric unit.
690 Monomeric FICD^{L258D} and dimeric wild-type FICD ± ATP, are coloured as indicated.
691 Glu234, ATP (and Mg, where applicable), are shown as sticks (or green spheres). The
692 inhibitory alpha helix (α_{inh}) and gross domain architecture is annotated. Note the only
693 significant deviation in tertiary structure is the flipping of the TPR domain in the
694 FICD^{L258D}:ATP structure. The FICD:Apo structure is from PDB: 4U0U. See [Figure](#)
695 [S5A](#).

696 **B)** Cocrystallisation of FICD variants with MgATP results in electron densities for
697 nucleotide and the inhibitory Glu234. Unbiased polder (OMIT) maps for ATP (± Mg)
698 and Glu234 are shown as blue and purple meshes, respectively. *(i)* The wild-type dimer
699 FICD structure displays a lack of density corresponding to a Mg²⁺ ion. The ATP density
700 is contoured at 3.5 σ and the Glu234 at 5.0 σ . *(ii)* The dimeric dimer relay mutant
701 FICD^{K256A} displays a clear MgATP density up to and including the γ -phosphate
702 phosphorous atom. The ATP density and Glu234 densities are both contoured at 3.0 σ .
703 *(iii)* Monomeric FICD^{L258D} shows a clear MgATP density. The ATP density is
704 contoured at 3.0 σ and the Glu234 at 5.0 σ . All residues and water molecules interacting
705 with ATP (± Mg) are shown as sticks and coloured by heteroatom. Mg²⁺ coordination
706 complex pseudo-bonds are shown in purple dashed lines. See [Figure S5B](#).

707 **C)** Unlike the monomeric or the dimer relay FICD mutants, dimeric wild-type FICD
708 binds ATP in a configuration that would prevent BiP substrate AMPylation. The
709 position of the α -phosphate in the FICD:ATP structure would preclude in-line
710 nucleophilic attack (see [Figure S5C-D](#)). The left panel represents the superposition of
711 the structures in the upper panel of *(B)*, with ATP interacting residues shown as sticks
712 and annotated. Only Glu234 deviates significantly in sidechain position. Note,
713 however, that the FICD:ATP His363 sidechain is also flipped, forming a hydrogen bond
714 to a ribose interacting water (see *Bi*). Mg²⁺ and ATP are coloured to match the
715 corresponding ribbons. Active site waters are omitted for clarity. Distances are
716 indicated by dashed black lines. The inset is a blow-up displaying distances *i-iv* between
717 the γ -phosphates and Glu234 residues. Note, distances *i* and *ii* are derived from the γ -

718 phosphate and Glu234 of different superimposed structures. Distances between
719 Val316(C γ 1) and the corresponding P α are shown in the right-hand side panel. See
720 [Figures S6-7](#).

721

722 **Figure 6**

723 **ATP destabilises the pre-AMPylation complex and the FICD dimer**

724 **A)** BioLayer interferometry (BLI) derived association and dissociation traces of
725 monomeric FICD^{L258D-H363A} (mFICD^{H363A}) or dimeric FICD^{H363A} (dFICD^{H363A}) from
726 immobilized biotinylated BiP^{T229A-V461F} in absence or presence of nucleotides. Unless
727 indicated (*) BiP was saturated with ATP before exposure to FICD variants. A
728 representative experiment of three independent repetitions is shown. See [Figure S8A-](#)
729 [B](#).

730 **B)** BLI dissociation traces of proteins as in (A). At $t = 0$ a pre-assembled complex of
731 immobilised, ATP-saturated BiP and the indicated FICD proteins (associated without
732 ATP) were transferred into a solution without or with ATP, as indicated. A
733 representative experiment is shown and the biphasic dissociation kinetics are quantified
734 in (C) and (D). Full association and dissociation traces are shown in [Figure S8C](#).

735 **C)** Graph of the slow dissociation rates ($k_{\text{off,slow}}$) of monomeric FICD from BiP:ATP as
736 shown in (B). Bars represent mean values \pm SD of three independent experiments.

737 **D)** The ATP-induced fold change in the percentage of the dissociation phase attributed
738 to a fast dissociation (%Fast), $k_{\text{off,fast}}$, and $k_{\text{off,slow}}$ derived from the data represented in
739 (B). Bars show mean values \pm SD of three independent experiments. See [Figure S8D](#).

740 **E)** BLI dissociation traces of the FICD dimer at different nucleotide concentration. At
741 $t = 0$ the species on the biosensor is a heterodimer of N-terminally biotinylated and an
742 exchangeable, non-biotinylated FICD. Dissociation was conducted \pm ligands (5 mM),
743 as indicated. A representative experiment of four independent repeats, with mono-
744 exponential fits are shown. See [Figure S8E](#) for raw data.

745 **F)** Cartoon schematic of the BLI assay workflow used to derive data presented in (E)
746 and [Figure S8E](#).

747 **G)** Quantification of the off rates derived from (E). ATP, but no ADP, significantly
748 increases the dimer dissociation rate [**: $p < 0.01$, by Tukey test; n.s.: not
749 significant]. Data shown is the mean \pm SD of four independent experiments.

750 **Figure 7**

751 A proposed model of an oligomerisation state-dependent switch in FICD bifunctional
752 active site. Under conditions of ER-stress the dimeric form FICD is favoured (right
753 hand side). Dimeric FICD cannot bind ATP in an AMPylation competent mode but can
754 efficiently catalyse deAMPylation of BiP-AMP (thereby remobilising BiP back into the
755 chaperone cycle). A decrease in unfolded protein load in the ER, possibly associated
756 with a decreased ER ADP/ATP ratio, shifts the FICD monomer-dimer equilibrium
757 towards monomeric FICD. Monomeric FICD can bind MgATP in an AMPylation
758 competent conformation and, as such, AMPylate and inactivate surplus BiP.

759 **Table 1:** Data Collection and refinement statistics. Values in parentheses correspond to the highest-resolution shell, with the following exceptions:
760 *The number of molecules in the biological unit is shown in parentheses; **MolProbity percentile score is shown in parentheses (100th percentile
761 is the best among structures of comparable resolutions, 0th percentile is the worst).
762

| | FICD:ATP | FICD^{K256S}:Apo | FICD^{K256A}:MgATP | FICD^{L258D}:Apo | FICD^{L258D}:MgATP | FICD^{L258D}:MgAMP -PNP |
|-----------------------------------|--|---|---|---------------------------------|-----------------------------------|--|
| Data collection | | | | | | |
| Synchrotron stations | DLS I04 | DLS I04 | DLS I03 | DLS I04 | DLS I03 | DLS I03 |
| Space group | <i>P</i> 2 ₁ 2 ₁ 2 | <i>P</i> 22 ₁ 2 ₁ | <i>P</i> 22 ₁ 2 ₁ | <i>P</i> 3 ₁ 21 | <i>P</i> 6 ₄ 22 | <i>P</i> 6 ₄ 22 |
| Molecules in a.u.* | 2 (2) | 1 (2) | 1 (2) | 1 (1) | 1 (1) | 1 (1) |
| a,b,c; Å | 77.67, 107.65, 132.60 | 43.82, 76.51, 131.97 | 41.90, 73.98, 134.04 | 118.14, 118.14, 79.55 | 186.84, 186.84, 76.84 | 186.36, 186.36, 77.10 |
| $\alpha, \beta, \gamma; ^\circ$ | 90.00, 90.00, 90.00 | 90.00, 90.00, 90.00 | 90.00, 90.00, 90.00 | 90.00, 90.00, 120.00 | 90.00, 90.00, 120.00 | 90.00, 90.00, 120.00 |
| Resolution, Å | 83.58-2.70 (2.83-2.70) | 65.99-2.25 (2.32-2.25) | 134.04-2.32 (2.41- 2.32) | 62.80-2.65 (2.72- 2.65) | 93.42-2.54 (2.65- 2.54) | 93.18-2.31 (2.39- 2.31) |
| R_{merge} | 0.163 (0.717) | 0.109 (0.385) | 0.107 (0.636) | 0.176 (0.856) | 0.167 (1.009) | 0.071 (0.611) |
| $\langle I/\sigma(I) \rangle$ | 19.2 (1.8) | 6.8 (2.4) | 5.6 (1.0) | 8.6 (2.2) | 13.0 (2.5) | 10.3 (1.8) |
| CC1/2 | 0.999 (0.720) | 0.993 (0.547) | 0.995 (0.567) | 0.996 (0.549) | 0.999 (0.503) | 0.998 (0.523) |
| No. of unique reflections | 31293 (4091) | 21825 (1978) | 18543 (1712) | 18963 (1380) | 26617 (3188) | 34573 (3351) |
| Completeness, % | 100.0 (100.0) | 99.9 (99.5) | 99.4 (97.3) | 100.0 (100.0) | 100.0 (100.0) | 99.4 (99.1) |
| Redundancy | 6.4 (6.5) | 4.4 (4.4) | 3.7 (3.7) | 9.7 (10.0) | 16.1 (16.5) | 4.6 (4.6) |
| Refinement | | | | | | |
| $R_{\text{work}}/R_{\text{free}}$ | 0.280 / 0.319 | 0.208 / 0.259 | 0.282 / 0.325 | 0.228 / 0.283 | 0.232 / 0.252 | 0.214 / 0.251 |
| No. of atoms (non-H) | 5650 | 2851 | 2731 | 2951 | 2828 | 2940 |
| Average B-factors, Å ² | 55.3 | 42.5 | 54.6 | 50.9 | 58.2 | 56.4 |
| RMS Bond lengths, Å | 0.002 | 0.003 | 0.003 | 0.003 | 0.002 | 0.003 |

| | | | | | | |
|---------------------------------|---------------------------|---------------------------|---------------------------|---------------------------|---------------------------|---------------------------|
| RMS Bond angles, ° | 1.142 | 1.180 | 0.763 | 1.222 | 1.127 | 1.170 |
| Ramachandran favoured region, % | 96.5 | 98.5 | 98.2 | 97.9 | 98.5 | 99.4 |
| Ramachandran outliers, % | 0 | 0 | 0 | 0 | 0 | 0 |
| MolProbity score** | 1.33 (100 th) | 0.86 (100 th) | 0.74 (100 th) | 0.99 (100 th) | 0.97 (100 th) | 0.99 (100 th) |
| PDB code | 6i7g | 6i7h | 6i7i | 6i7j | 6i7k | 6i7l |

763

764 **Figure S1**

765 **Low-level expression facilitates AMPylation in vivo and FICD mutations are able**
766 **to disrupt the tight dimer formed in solution.**

767 **A)** Schematic representation of the domain organization of FICD and the shorter protein
768 fragment used for in vitro experiments. The transmembrane domain (blue), the TPR
769 domain (orange), the α -helical linker (green), the Fic domain (purple) and the core Fic
770 domain (deep purple) including the active site motif are indicated.

771 **B-C)** Characterization of CHO-K1 *FICD*^{-/-} UPR reporter clones stably expressing wild-
772 type FICD. **(B)** Flow cytometry analysis of CHO-K1 *FICD*^{-/-} UPR reporter clones
773 stably-expressing mCherry and FICD. Clones were selected based on mCherry signal,
774 assuming a direct correlation with FICD expression levels. **(C)** Immunoblot of
775 endogenous BiP from CHO-K1 *FICD*^{-/-} clones shown in *(B)* exposed to cycloheximide
776 as in [Figure 1A](#). Note that only clone 10, with an intermediate mCherry signal, showed
777 detectable accumulation of AMPylated BiP.

778 **D-E)** Size-exclusion chromatography (SEC) analysis of wild-type and mutant FICD
779 proteins. **(D)** SEC elution profiles with FICD proteins at the indicated concentrations.
780 Black dots mark the position of the elution peaks. Dotted lines mark the approximate
781 elution peak times for dimeric (10.2 min) and monomeric (11.4 min) FICD,
782 respectively. **(E)** Plot of the elution peak times from *(D)* as a function of protein
783 concentration. With the exception of FICD^{G299S} (*; a mutation that shifts the elution
784 time relative to the monomer) best-fit monomer-dimer association curves are shown
785 with the top plateau constrained to the monomer elution time (11.4 min). Approximate
786 dimerisation K_{As} were derived and are shown in the figure key for the different partially
787 monomerising mutants (with 95% confidence intervals). Note that FICD^{L258D} eluted as
788 a monomer and wild-type FICD principally as a dimer at all concentrations tested (0.2-
789 50 μ M). Conversely, FICD^{G299S} and non-oxidized FICD^{A252C-C421S} formed much
790 weaker dimers. As in *(D)* the monomer and dimer elution times are represented by
791 dotted (horizontal) lines.

792 **F-G)** Analysis of FICD by analytical ultracentrifugation. Overlays of $c(s)$ distributions
793 of **(F)** wild-type FICD and **(G)** FICD^{L258D} are shown in units of experimental s -values.
794 A signal-weighted isotherm for the wild-type protein ([Figure 1E](#)) was generated from
795 integration of the titration series distributions.

796 **Figure S2**

797 **Monomerisation inhibits deAMPylation and markedly stimulates FICD**
798 **AMPylation activity.**

799 **A)** Summary of deAMPylation rates of wild-type and mutant FICD proteins. Shown
800 are deAMPylation rates of BiP^{V461F}-AMP^{FAM} by the indicated FICD proteins (at 0.75
801 μ M or 7.5 μ M) as detected by a change in fluorescence polarisation. Mean values \pm SD
802 of the normalized raw data fitted to a single-exponential decay function of at least four
803 independent measurements are presented.

804 **B-C)** The effect of FICD overexpression on a UPR reporter. **(B)** Flow cytometry
805 analysis of wild-type and *FICD*^{-/-} CHO-K1 *CHOP::GFP* UPR reporter cells transfected
806 with plasmids encoding wild-type or the indicated FICD derivatives and a mCherry
807 transfection marker. Shown are the median values \pm SD of the GFP fluorescence signal
808 of mCherry-positive cells from three independent experiments (fold change relative to
809 wild-type cells transfected with a plasmid encoding mCherry alone). Note that only
810 Glu234Gly-containing, deAMPylation-deficient FICDs activate the reporter. **(C)** Flow
811 cytometry raw data of a representative experiment quantified in *(B)*.

812 **D)** AMP production by FICD dimer interface or relay mutants is BiP dependent. AMP
813 production in the presence of [α -³²P]-ATP was measured by TLC and autoradiography
814 (as in [Figure 2B](#)). Plotted below are mean AMP values \pm SD (n = 3).

815 **E-G)** Characterization of covalently linked *s-sFICD*^{A252C-H363A-C421S} dimers – a trap for
816 BiP-AMP. **(E)** Coomassie-stained, SDS-PAGE gel of the indicated FICD proteins. **(F)**
817 Size-exclusion chromatography elution profiles of wild-type FICD and covalently
818 linked *s-sFICD*^{A252C-H363A-C421S} (trap) dimers at 20 μ M, as in [Figure 1D](#). Note that the
819 oxidised trap elutes, like the wild-type FICD, as a dimer. **(G)** BioLayer interferometry
820 (BLI) derived association and dissociation traces of the indicated FICD proteins (in
821 solution) from immobilized AMPylated (BiP-AMP) or unmodified BiP. The trap (*s-*
822 *sFICD*^{A252C-H363A-C421S}) and *FICD*^{H363A} had indistinguishable tight interaction with BiP-
823 AMP (with low off rates). The interaction of BiP-AMP with monomeric *FICD*^{L258D-}
824 ^{H363A} was more transient. The interaction between these FICD variants and unmodified
825 BiP was further diminished.

826 **H)** Sequestration of AMPylated BiP by trap FICD analysed by SEC. Elution profiles
827 of in vitro AMPylation reactions containing the indicated components in the presence

828 or absence of covalently linked s-sFICD^{A252C-H363A-C421S} (trap) dimers to sequester the
829 AMPylated BiP product. Note that the trap forms a stable complex with BiP when
830 AMPylated by monomeric FICD^{L258D}. An early eluting species, representing a stable
831 complex between modified BiP and trap, only occurs in the reaction containing
832 AMPylation-active, monomeric FICD^{L258D} and ATP (bottom right panel, pink trace).
833 Here, BiP-mediated ATP hydrolysis and substrate interactions were discouraged by use
834 of a BiP^{T229A-V461F} double mutant.
835

836 **Figure S3**

837 **Non-disulphide-linked FICD^{A252C-C421S} shows enhanced AMPylation activity.**

838 **A)** Coomassie-stained, non-reducing SDS-PAGE gel of the indicated FICD proteins.

839 **B)** Size exclusion chromatography (SEC) elution profiles of FICD proteins injected at
840 a concentration of 20 μ M. Protein absorbance at 280 nm is plotted against elution time.

841 The elution times of protein standards are indicated as a reference. Note that wild-type
842 FICD, FICD^{C421S}, and oxidised s-sFICD^{A252C-C421S} co-elute as dimers. See [Figure S1D-](#)
843 [E](#).

844 **C)** Radioactive in vitro AMPylation reactions were performed as in the right hand side
845 panel of [Figure 3A](#), that is with the indicated FICD proteins under non-reducing
846 conditions in presence of covalently linked s-sFICD^{A252C-H363A-C421S} dimers (trap). Note
847 that the accumulation of modified BiP correlates with the FICD concentration. Less
848 modified BiP was produced by covalently-linked, oxidised s-sFICD^{A252C-C421S} dimers,
849 whereas more AMPylated BiP was generated in reactions containing non-oxidised
850 FICD^{A252C-C421S}. The trap, present at 5 μ M, co-migrates with the indicated FICD
851 enzyme and dominates the signal in the Coomassie stained gel (FICD/trap).

852 **D)** Time-dependent in vitro deAMPylation of fluorescent BiP^{V461F}-AMP^{FAM} by the
853 indicated FICD proteins (at 7.5 μ M) assayed by fluorescence polarisation (as in [Figure](#)
854 [2A](#)). A representative experiment (data points and fit curves) is shown and
855 deAMPylation rates are presented in [Figure S2A](#). Note that non-oxidised FICD^{A252C-}
856 ^{C421S} has very similar deAMPylation kinetics to the wild-type protein. This contrasts
857 with the oxidised form which displays a slight increase in deAMPylation rate ([Figure](#)
858 [3D and S2A](#)).

859

860 **Figure S4**

861 **FICD dimer relay mutants produce a pool of AMPylated BiP in vitro, and FICD**
862 **AMPylation activity correlates with increased flexibility.**

863 **A)** Radioactive in vitro AMPylation reactions with the indicated FICD proteins at the
864 indicated concentrations, [α -³²P]-ATP, and BiP^{T229A-V461F} were analysed by SDS-
865 PAGE. The radioactive signals were detected by autoradiography and proteins were
866 visualised by Coomassie staining. Note the enhanced production of AMPylated BiP in
867 the presence of dimer relay mutants, FICD^{K256S} and FICD^{E242A}, relative to the wild-type
868 protein and a further increase in the production of AMPylated BiP by the monomeric
869 FICD^{K256S-L256D} double mutant relative to the monomeric FICD^{L258D}. Also note the
870 auto-AMPylation signals of the monomeric FICDs at high enzyme concentration.

871 **B-C)** In vitro deAMPylation of fluorescent BiP^{V461F}-AMP^{FAM} by the indicated FICD
872 proteins (at 7.5 μ M) measured by fluorescence polarisation. A representative
873 experiment (data points and fit curves) is shown and rates are presented in [Figure S2A](#).
874 Note the impaired deAMPylation activity of the monomeric FICD^{K256S-L256D} double
875 mutant in (C).

876 **D)** DSF T_m analysis of wild-type (wt) and mutant FICD proteins in absence (Apo) or
877 presence of ATP or ADP. Nucleotide concentrations are given in parentheses. Non-
878 oxidised and oxidised forms of FICD^{A252C-C421S} were assayed in buffer lacking reducing
879 agent (which did not affect the T_m of wild-type FICD; not shown). Shown are the mean
880 T_m values \pm SD from three independent experiments. Note that FICD^{K256A} is more
881 stable than FICD^{K256S} but less than wild-type FICD. Furthermore, the stabilities of
882 oxidised and non-oxidised FICD^{C421S-A252C} relative to the wild-type correlate inversely
883 with their AMPylation activities ([Figure 3B](#)). The same data for the wild-type FICD,
884 FICD^{E242A}, FICD^{G299S}, FICD^{L258D} and FICD^{K256S-L258D} in the Apo state are presented in
885 [Figure 4E](#).

886 **E)** Plot of the increase in FICD melting temperature (ΔT_m) against ATP concentration
887 as measured by DSF (derived from [Figure 4F](#)). Note the similarity in the plot of
888 FICD^{L258D} (mFICD) and the wild-type dimer (dFICD); mFICD $K_{1/2}$ 2.5 ± 0.6 mM and
889 dFICD $K_{1/2}$ 3.2 ± 0.3 mM. Shown are mean ΔT_m values \pm SD of three independent
890 experiments with the best fit lines for a one site binding model.

891 **Figure S5**

892 **Monomerisation allows ATP to bind to FICD in a mode conducive to BiP**
893 **AMPylation.**

894 **A)** Mutation of the dimer relay residue Lys256 does not result in large conformational
895 changes in FICD. Shown is the alignment (residues 213-407) of the molecules in the
896 asymmetric unit. Structures are coloured as indicated. Glu234, ATP and Mg (where
897 applicable), are shown as sticks. The inhibitory alpha helix (α_{inh}) and gross domain
898 architecture is annotated. The FICD:Apo structure is from PDB: 4U0U.

899 **B)** Electron density of both MgAMPPNP and the inhibitory Glu234, from monomeric
900 FICD^{L258D} co-crystallized with MgAMPPNP. Unbiased polder (OMIT) maps are
901 shown in blue and purple meshes, contoured at 3.0 and 5.0 σ , respectively. All residues
902 and water molecules interacting with MgAMPPNP are shown as sticks and coloured
903 by heteroatom. Mg²⁺ coordination complex pseudo-bonds are shown in purple dashed
904 lines.

905 **C)** Unlike wild-type FICD, monomeric FICD^{L258D} binds ATP and ATP analogues in
906 an AMPylation competent conformation. The indicated structures and distances are
907 shown as in [Figure 5C](#), with ATP interacting residues shown as sticks and annotated.
908 The position of the α -phosphate relative to Val316 in the FICD:ATP structure (see
909 distances in right hand side panel) would preclude in-line nucleophilic attack (see D-
910 E). The inset is a blow-up displaying distances *i-iv* between the γ -phosphates and
911 Glu234 residues. A potentially significant difference in the Glu234 position between
912 the FICD^{L258D}:MgAMPPNP and FICD:ATP structures is apparent: hypothetical
913 distance *ii* (2.68 Å, between Glu234 of FICD:ATP and AMPPNP γ -phosphate of
914 FICD^{L258D}) is less favourable than the observed distance *iii* (2.94 Å, between the
915 AMPPNP γ -phosphate and Glu234 of FICD^{L258D}). Note, His363 of FICD:ATP is in a
916 non-optimal flip state to facilitate general base catalysis (see [Figure 5B](#)).

917 **D) (i)** The mode of ATP binding in wild-type dimeric FICD sterically occludes the
918 nucleophilic attack required for AMPylation. Shown are semi-opaque 3 Å centroids
919 centred on P α and Val316 (C γ 1). The putative BiP Thr518 nucleophile (depicted by the
920 cross) is positioned in-line with the scissile phosphoanhydride (parallel to the plane of
921 the paper) and 3 Å from P α . This nucleophile position lies within the Val316 centroid
922 (indicating a steric clash). For clarity, the FICD:ATP structure is overlaid with a thin

923 slice of the FICD:ATP structure in the plane of the P α -O3 α bond. **(ii)** In the monomeric
924 AMPylation-competent FICD^{L258D}:ATP structure the nucleophile lies outside the
925 Val316 centroid in proximity to His363 (the general base).

926 **E)** The ATP α -phosphates of monomer or dimer relay mutants are in the same position
927 as that competently bound to the AMPylation unrestrained dimeric FICD^{E234G}. Shown
928 are all AMPylation competent MgATP structures overlaid as in (C) and [Figure 5C](#). The
929 dimeric FICD^{E234G}:MgATP (dark blue, PDB: 4U07) is also included as a reference for
930 an active AMPylating enzyme.

931

932 **Figure S6**

933 **FICD crystallographic packing and dimer interface.**

934 **A)** The hydrogen bonding network connecting the dimer interface and enzyme active
935 site is maintained in the crystal structures of monomeric and Lys256 mutant FICDs. An
936 alignment of the hydrogen bond network linking the dimer interface to Glu234 in the
937 indicated structures is displayed (in the same view as [Figure 4A](#)). H-bonds are shown
938 in blue dashed lines. Where indicated, single molecules from the asymmetric unit
939 (underlined) are displayed with their respective symmetry mates (Sym1). Note, the
940 side-chains of Asp258 and (Sym1)Arg250 of the monomeric FICD^{L258D} (cocrystallised
941 with nucleotide) form a crystallographically induced inter-molecular H-bond (magenta
942 dashed line). The salt-bridges between the Glu234 and the Fic motif Arg374 (magenta
943 dashed lines) in the FICD^{L258D}:Apo and FICD^{K256S}:Apo structures, observed in other
944 inhibitory glutamate-containing Fic crystal structures, are also shown.

945 **B)** Dimer interface contacts are imposed crystallographically, and crystal packing
946 around the α_{inh} is similar in all FICD structures. FICDs with similar crystal packings are
947 grouped into panels (*i-iv*). The inhibitory alpha helix (α_{inh}) is denoted with an asterisk
948 (*) and Glu234s are shown as sticks. The wild-type dimeric FICD:Apo structure
949 (FICD:Apo; PDB:4U0U) is provided in all panels for reference. Where a single FICD
950 molecule constituted the asymmetric unit, symmetry mates within 4 Å of its dimer
951 interface (Sym1) or 4 Å of its inhibitory helix region (Sym2/3) are also displayed. Note
952 that crystals of the Lys256 mutants (*ii*) contain a single molecule in their asymmetric
953 unit but are packed as dimers, crystallographically reconstituting the dimeric biological
954 unit. The asymmetric unit of FICD^{L258D} bound to ATP (or an ATP analogue) (*iv*)
955 contains a single molecule and thus corresponds to the biological unit of this
956 monomeric protein. However, packing against its symmetry mates (Sym1),
957 crystallographically reconstitutes a dimer interface that is highly similar, but not
958 identical, to that observed in the wild-type protein (see Asp258 and (Sym1)Arg250 in
959 [S6A](#), above). Sym2 in (*iv*) serves to highlight the replacement of the flipped out TPR
960 domain with the flipped out TPR domain from a symmetry mate. In (*iv*) there are no
961 crystal contacts in the vicinity of the α_{inh} .

962

963 **Figure S7**

964 **AMPylation activity correlates with enhanced flexibility of the dimer interface**
965 **and Glu234.**

966 The residue average B-factors, for the four FICD complexes cocrystallised with ATP,
967 are shown [in (*i-iv*)] with a cold to hot colour code. They display a trend of increasing
968 B-factors in the dimer interface and in the inhibitory glutamate region. This increase in
969 B-factor is indicative of increasing flexibility and correlates with greater AMPylation
970 activity of the corresponding FICD. All of these structures have almost identical dimer
971 packing in their respective crystals and limited crystal contacts around the inhibitory
972 helix (see [Figure S6](#)). Note, structure averaged B-factors are comparable (see [Table 1](#)).
973 For clarity, the TPR domain (up to residue 182) is not shown.

974

975 **Figure S8**

976 **ATP negatively modulates pre-AMPylation complex and FICD dimer stability.**

977 **A)** Immobilised BiP responds allosterically to, is saturated by and retains ATP for the
978 duration of BLI kinetic assays. BLI traces of the interaction between FICD^{L258D-H363A}
979 and immobilised biotinylated BiP^{T229A-V461F} in different nucleotide states. Before
980 exposure to FICD^{L258D-H363A} immobilised BiP:Apo was subjected to two consecutive
981 incubation steps (activation and wash) in the presence or absence of ATP as indicated.
982 FICD association and dissociation steps (shown) were then conducted in a nucleotide
983 (Nt.)-free solution. Note that BiP only interacts with FICD^{L258D-H363A} when pre-
984 saturated with ATP. Importantly, ATP pre-bound BiP retains its affinity for FICD^{L258D-}
985 ^{H363A} even if subsequently washed in a buffer lacking ATP (compare red and green
986 traces). Thus BiP retains its bound ATP for the duration of the kinetic experiment,
987 experimentally uncoupling the effect of nucleotide on the FICD analyte from its effect
988 on the immobilised BiP ligand.

989 **B)** Cartoon schematic of the BLI assays presented in [Figures 6A-B](#). The pre-
990 AMPylation complex is formed between the immobilised BiP:ATP ‘ligand’ and the
991 FICD ‘analyte’.

992 **C)** The BLI association and dissociation traces from [Figure 6B](#) are shown. The
993 immobilised biotinylated BiP^{T229A-V461F} was saturated with ATP and then exposed to
994 nucleotide-free FICDs. Dissociation was performed in absence or presence of ATP, as
995 indicated. [mFICD^{H363A}: FICD^{L258D-H363A}, dFICD^{H363A}: FICD^{H363A}].

996 **D)** Quantification of the biphasic exponential decay fitting of dissociation traces shown
997 in [Figure 6B](#). Relative ATP-induced changes of these kinetic parameters are given in
998 [Figure 6D](#). Shown are mean values \pm SD from three independent experiments. Note the
999 greater relative contribution of fast dissociation of mFICD in presence of ATP versus
1000 absence.

1001 **E)** Representative BLI traces of an FICD dimer dissociation experiment plotted in
1002 [Figure 6E](#). The legend indicates the form of unlabelled FICD incubated with the N-
1003 terminally biotinylated FICD (at a 100-fold molar excess, prior to biosensor loading)
1004 and also the ligand present in the dissociation buffer (at 5 mM) if applicable. Note,
1005 probes loaded with biotinylated FICD incubated with mFICD^{H363A} act as controls for

1006 non-specific association and dissociation signals, these were subtracted from the
1007 respective dFICD^{H363A} traces in [Figure 6E](#).

1008 **Table S1**

1009 Crystallisation conditions. Where applicable the crystallisation conditions (and seed dilution) of the crystals used for micro-seeding are also shown.

1010 Note, PEG percentage is given in w/v and EtOH percentage in v/v.

| Dataset | PDB Code | Crystallisation Condition (<i>Protein:Seeds:Well Solution (nl)</i>) | Seed Protein | Seed Crystal Conditions (<i>Seed Dilution</i>) |
|----------------------------------|-----------------|---|-----------------------------|--|
| FICD:ATP | 6i7g | 0.1 M Tris pH 7.5; 20% PEG 300; 5% PEG8K; 10% Glycerol (150:50:100) | FICD | 0.2 M (NH ₄) ₂ SO ₄ , 0.1 M NaCacodylate, 30% PEG 8000 (1/3) |
| FICD ^{K256S} :Apo | 6i7h | 0.1 M Tris pH 8.5; 0.05 M MgCl ₂ ; 40% EtOH (200:0:100) | N/A | N/A |
| FICD ^{K256A} :MgATP | 6i7i | 0.1 M Bis-Tris pH 6.5; 0.2 M MgCl ₂ ; 25% PEG3350 (100:25:100) | FICD ^{K256A} | 0.1 M Na ₃ Citrate pH 5.5, 40% PEG 600 (1/10) |
| FICD ^{L258D} :Apo | 6i7j | 0.1 M Tris pH 8.5; 2.0 M (NH ₄) ₂ SO ₄ (150:50:100) | FICD ^{L258D} | 0.1 M Tris pH 8.5, 0.2 M Li ₂ SO ₄ , 40% PEG 4000 (1/2) |
| FICD ^{L258D} :MgATP | 6i7k | 1.0 M NaCl; 10% EtOH (150:50:200) | FICD ^{L258D-H363A} | 0.1 M HEPES pH 7.5, 1 M NaOAc (1/100) |
| FICD ^{L258D} :MgAMP-PNP | 6i7l | 1.5 M NaCl; 10% EtOH (150:50:200) | FICD ^{K256A} | 0.1 M Na ₃ Citrate pH 5.5, 40% PEG 600 (1/500) |

1011

1012 **Table S2**

1013 List of plasmids used, their lab names, description, their corresponding label and references.

1014 **Materials and Methods**

1015

1016 **Plasmid construction**

1017 The plasmids used in this study have been described previously or were generated by
1018 standard molecular cloning procedures and are listed in [Table S2](#).

1019

1020 **Cell lines**

1021 All cells were grown on tissue culture dishes or multi-well plates (Corning) at 37 °C
1022 and 5% CO₂. CHO-K1 cells (ATCC CCL-61) were phenotypically validated as proline
1023 auxotrophs and their *Cricetulus griseus* origin was confirmed by genomic sequencing.
1024 *CHOP::GFP* and *XBPIs::Turquoise* reporters were introduced sequentially under
1025 G418 and puromycin selection to generate the previously-described derivative CHO-
1026 K1 S21 clone (Sekine *et al*, 2016). The cells were cultured in Nutrient mixture F-12
1027 Ham (Sigma) supplemented with 10% (v/v) serum (FetalClone II; HyClone), 1 x
1028 Penicillin-Streptomycin (Sigma), and 2 mM L-glutamine (Sigma). The CHO-K1 *FICD*^{-/-}
1029 cell line used in this study was described previously (Preissler *et al*, 2015b). HEK293T
1030 cells (ATCC CRL-3216) were cultured in Dulbecco's Modified Eagle's Medium
1031 (Sigma) supplemented as described above. Cell lines were subjected to random testing
1032 for mycoplasma contamination using the MycoAlert Mycoplasma Detection Kit
1033 (Lonza).

1034 Experiments were performed at cell densities of 60-90% confluence. Where indicated,
1035 cells were treated with cycloheximide (Sigma) at 100 µg/ml diluted with fresh, pre-
1036 warmed medium and then applied to the cells by medium exchange.

1037

1038 **Mammalian cell lysates**

1039 Cell lysis was performed as described in (Preissler *et al*, 2015a) with modifications. In
1040 brief, mammalian cells were cultured on 10 cm dishes and treated as indicated and/or
1041 transfected using Lipofectamine LTX with 5 µg plasmid DNA, and allowed to grow
1042 for 24 to 40 h. Before lysis, the dishes were placed on ice, washed with ice-cold PBS,
1043 and cells were detached in PBS containing 1 mM ethylenediaminetetraacetic acid

1044 (EDTA) using a cell scraper. The cells were sedimented for 5 min at $370 \times g$ at 4°C
1045 and lysed in HG lysis buffer [20 mM HEPES-KOH pH 7.4, 150 mM NaCl, 2 mM
1046 MgCl_2 , 10 mM D-glucose, 10% (v/v) glycerol, 1% (v/v) Triton X-100] containing
1047 protease inhibitors (2 mM phenylmethylsulphonyl fluoride (PMSF), 4 $\mu\text{g/ml}$ pepstatin,
1048 4 $\mu\text{g/ml}$ leupeptin, 8 $\mu\text{g/ml}$ aprotinin) with 100 U/ml hexokinase (from *Saccharomyces*
1049 *cerevisiae* Type F-300; Sigma) for 10 min on ice. The lysates were cleared for 10 min
1050 at $21,000 \times g$ at 4°C . Bio-Rad protein assay reagent (BioRad) was used to determine
1051 the protein concentrations of lysates. For analysis by SDS-PAGE, SDS sample buffer
1052 was added to the lysates and proteins were denatured by heating for 10 min at 70°C
1053 before separation on 12.5% SDS polyacrylamide gels. To detect endogenous BiP by
1054 native-PAGE the lysate samples were loaded immediately on native gels (see below).

1055

1056 **Native polyacrylamide gel electrophoresis (native-PAGE)**

1057 Non-denaturing native-PAGE was performed as described (Preissler *et al.*, 2015a).
1058 Briefly, Tris-glycine polyacrylamide gels (4.5% stacking gel and a 7.5% separation gel)
1059 were used to separate proteins from mammalian cell lysates to detect BiP monomers
1060 and oligomers. The separation was performed in running buffer (25 mM Tris, 192 mM
1061 glycine, pH ~ 8.8) at 120 V for 2 h. Afterwards, the proteins were transferred to a
1062 polyvinylidene difluoride (PVDF) membrane in blotting buffer (48 mM Tris, 39 mM
1063 glycine; pH ~ 9.2) supplemented with 0.04 (w/v) SDS for 16 h at 30 V for
1064 immunodetection. The membrane was washed for 20 minutes in blotting buffer
1065 (without SDS) supplemented with 20% (v/v) methanol before blocking. Volumes of
1066 lysates corresponding to 30 μg of total protein were loaded per lane to detect
1067 endogenous BiP from cell lysates by immunoblotting.

1068

1069 **Streptavidin pull-down and FLAG immunoprecipitation**

1070 To analyse the formation of FICD dimers in vivo ([Figure 1B](#)), CHO-K1 cells were
1071 transfected with 4 μg plasmid DNA encoding His₆-AviTag-FICD (UK 2275) or His₆-
1072 AviTag-FICD^{L258D} (UK 2319) and FLAG-FICD (UK 2276) or FLAG-FICD^{L258D} (UK
1073 2318), and 4 μg plasmid DNA encoding BirA (in order to keep the final amount of
1074 plasmid DNA the same, an empty pCEFL plasmid was used; [Table S2](#)) as described
1075 above. 24 h before lysis the medium was exchanged to medium containing 50 μM

1076 Biotin (Molecular Probes). For streptavidin pull-down of His₆-AviTag-FICD, CHO-K1
1077 cells were transfected and allowed to grow for approximately 40 h before lysis in lysis
1078 buffer [50 mM Tris-HCl pH 7.4, 150 mM NaCl, 1% (v/v) Triton X-100, 10% (v/v)
1079 glycerol] supplemented with protease inhibitors. The lysates were cleared twice,
1080 normalized and equal volumes of the lysates were incubated with 50 µl Dynabeads
1081 (MyOne Streptavidin C1, Life Technologies) for 60 to 90 min at 4 °C, rotating. The
1082 beads were then recovered by centrifugation for 1 min at 200 × g and by placing the
1083 tube in a magnetic separation stand. They were then washed three times at 25 °C with
1084 RIPA buffer [50 mM Tris-HCl pH 8.0, 150 mM NaCl, 1% (v/v) Triton X-100, 0.5%
1085 (v/v) sodium deoxycholate, 0.1% (v/v) SDS] supplemented with protease inhibitors.
1086 Bound proteins were eluted in 25 µl urea sample buffer [8 M urea, 1.36% (v/v) SDS,
1087 12% (v/v) glycerol, 40 mM Tris-HCl pH 6.8, 0.002% (w/v) bromophenol blue, 100
1088 mM DTT] and heating for 10 min at 70 °C. Equal volumes of the samples were loaded
1089 on a 12.5% SDS polyacrylamide gel and His₆-AviTag-FICD and FLAG-FICD were
1090 detected by immunoblotting. Samples of the normalized lysates (60 µg) were loaded as
1091 an ‘input’ control.

1092 For the reciprocal experiment, FLAG M2 immunoprecipitation of FLAG-FICD, equal
1093 volumes of the cleared and normalized lysates were incubated with 20 µl of Anti-FLAG
1094 M2 affinity gel (Sigma) for 60 to 90 min at 4 °C, rotating. The beads were then
1095 recovered by centrifugation for 1 min at 5,000 × g and washed three times with RIPA
1096 buffer. The proteins were eluted in 35 µl 2 × SDS sample buffer (without DTT) for 10
1097 min at 70 °C. The beads were then sedimented and the supernatants were transferred to
1098 new tubes to which 50 mM DTT was added. Equal sample volumes were analysed by
1099 SDS-PAGE and immunoblotting as described above.

1100

1101 **Immunoblot analysis**

1102 After separation by SDS-PAGE or native-PAGE (see above) the proteins were
1103 transferred onto PVDF membranes. The membranes were blocked with 5% (w/v) dried
1104 skimmed milk in TBS (25 mM Tris-HCl pH 7.5, 150 mM NaCl) and incubated with
1105 primary antibodies followed by IRDye fluorescently labelled secondary antibodies (LI-
1106 COR). The membranes were scanned with an Odyssey near-infrared imager (LI-COR).
1107 Primary antibodies and antisera against hamster BiP [chicken anti-BiP (Avezov *et al*,

1108 2013)], eIF2 α [mouse anti-eIF2 α (Scorsone *et al*, 1987)], FICD [chicken anti-FICD
1109 (Preissler *et al*, 2015b)], monoclonal anti-FLAG M2 (Sigma), and IRDye 800CW
1110 Streptavidin (LI-COR) were used.

1111

1112 **Flow cytometry**

1113 FICD (wild-type and mutants) over-expression-dependent induction of unfolded
1114 protein response signalling was analysed by transient transfection of wild-type and
1115 *FICD*^{-/-} *CHOP::GFP* CHO-K1 UPR reporter cell lines with plasmid DNA encoding
1116 the FICD protein and mCherry as a transfection marker, using Lipofectamine LTX as
1117 described previously (Preissler *et al*, 2015b). 0.5 μ g DNA was used in [Figure S2B-C](#) to
1118 transfect cells growing in 12-well plates. 40 h after transfection the cells were washed
1119 with PBS and collected in PBS containing 4 mM EDTA, and single cell fluorescent
1120 signals (20,000/sample) were analysed by dual-channel flow cytometry with an
1121 LSRFortessa cell analyser (BD Biosciences). GFP and mCherry fluorescence was
1122 detected with excitation laser 488 nm, filter 530/30, and excitation laser 561, filter
1123 610/20, respectively. Data were processed using FlowJo and median reporter (in Q1
1124 and Q2) analysis was performed using Prism 6.0e (GraphPad).

1125

1126 **Production of VSV-G retrovirus in HEK293T cells and infection of CHO-K1 cells**

1127 In an attempt to establish BiP AMPylation in *FICD*^{-/-} cells ([Figure 1A](#)), cells were
1128 targeted with retrovirus expressing FICD (incorporating the naturally-occurring
1129 repressive uORF found in its cDNA) and mCherry. HEK293T cells were split onto 6
1130 cm dishes 24 h prior to co-transfection of pBABE-mCherry plasmid encoding FICD
1131 (UK 1939; [Table S2](#)) with VSV-G retroviral packaging vectors, using TransIT-293
1132 Transfection Reagent (Mirus) according to the manufacturer's instructions. 16 h after
1133 transfection, medium was changed to medium supplemented with 1% (w/v) BSA
1134 (Sigma). Retroviral infections were performed following a 24 h incubation by diluting
1135 0.45 μ m filter-sterilized cell culture supernatants at a 1:1 ratio into CHO-K1 cell
1136 medium supplemented with 10 μ g/ml polybrene (8 ml final volume) and adding this
1137 preparation to *FICD*^{-/-} CHO-K1 cells (1 x 10⁶ cells seeded onto 10 cm dishes 24 h prior
1138 to infection). Infections proceeded for 8 h, after which viral supernatant was replaced
1139 with fresh medium. 48 h later, the cells were split into four 10 cm dishes. Five days

1140 after transfection, single cells were sorted according to their mCherry intensity.
1141 Selected clones were expanded and analysed by flow cytometry (to assess mCherry
1142 intensity) and native-PAGE (to check for BiP AMPylation).

1143

1144 **Protein purification**

1145 FICD

1146 Wild-type and mutant human FICD proteins (aa 104-445) were expressed as His₆-Smt3
1147 fusion constructs in T7 Express *lysY/I^q* (NEB) *E. coli* cells. The cells were grown in LB
1148 medium (usually 6 l per construct) containing 50 µg/ml kanamycin at 37 °C to an
1149 optical density (OD_{600nm}) of 0.6 and then shifted to 18 °C for 20 min, followed by
1150 induction of protein expression with 0.5 mM isopropylthio β-D-1-galactopyranoside
1151 (IPTG). The cultures were further incubated for 16 h at 18 °C, harvested, and lysed with
1152 a high-pressure homogenizer (EmulsiFlex-C3; Avestin) in buffer A [25 mM Tris-HCl
1153 pH 8.0, 500 mM NaCl, 40 mM imidazole, 1 mM MgCl₂, 0.1 mM tris(2-
1154 carboxyethyl)phosphine (TCEP)] containing protease inhibitors [2 mM PMSEF, 4 µg/ml
1155 pepstatin, 4 µg/ml leupeptin, 8 µg/ml aprotinin], 0.1 mg/ml DNaseI, and 20 µg/ml
1156 RNaseA. The lysates were centrifuged for 30 min at 45,000 × *g* and incubated with 1
1157 ml of Ni-NTA agarose (Qiagen) per 1 l expression culture, for 30 min rotating at 4 °C.
1158 Afterwards, the beads were transferred to a gravity-flow Econo column (49 ml volume;
1159 BioRad), washed with five column volumes (CV) buffer A without MgCl₂ and buffer
1160 B (25 mM Tris-HCl pH 8.0, 150 mM NaCl, 10 mM imidazole, 0.1 mM TCEP). The
1161 beads were further washed sequentially with buffer B sequentially supplemented with
1162 (i) 1 M NaCl, (ii) 10 mM MgCl₂ + 5 mM ATP and (iii) 0.5 M Tris-HCl pH 8.0 [each 5
1163 CV], followed by 2 CV TNT-Iz10 (25 mM Tris-HCl pH 8.0, 150 mM NaCl, 1 mM
1164 TCEP, 10 mM imidazole). Proteins were eluted by on-column cleavage with 1.5 µg/ml
1165 Ulp1 protease carrying a C-terminal StrepII-tag [Ulp1-StrepII (UK 1983)] in 1 bed
1166 volume TNT-Iz10 overnight at 4 °C. The eluate was collected, retained cleavage
1167 products were washed off the beads with TNT-Iz10, and all fractions were pooled. The
1168 total eluate was diluted 1:2 with 25 mM Tris-HCl pH 8.0 and further purified by anion
1169 exchange chromatography using a 6 ml RESOURCE Q column (GE Healthcare)
1170 equilibrated in 95% AEX-A (25 mM Tris-HCl pH 8.0, 25 mM NaCl) and 5% AEX-B
1171 (25 mM Tris-HCl, 1 M NaCl). Proteins were eluted by applying a gradient from 5-30%

1172 AEX-B in 20 CV at 3 ml/min. Fractions of elution peaks (absorbance at 280 nm, $A_{280\text{nm}}$)
1173 corresponding to monomeric or dimeric FICD were pooled and concentrated using 30
1174 kDa MWCO centrifugal filters (Amicon Ultra; Merck Millipore) in the presence of 1
1175 mM TCEP. The proteins were then subjected to size-exclusion chromatography using
1176 a HiLoad 16/60 Superdex 200 prep grade column (GE Healthcare) equilibrated in SEC
1177 buffer (25 mM Tris-HCl pH 8.0, 150 mM NaCl). Peaks corresponding to monomeric
1178 or dimeric FICD were supplemented with 1 mM TCEP, concentrated ($> 120 \mu\text{M}$), and
1179 frozen in aliquots.

1180 BiP

1181 Mutant Chinese hamster BiP proteins with an N-terminal His₆-tag were purified as
1182 described before with modifications (Preissler *et al*, 2017b). Proteins were expressed
1183 in M15 *Escherichia coli* (*E. coli*) cells (Qiagen). The bacterial cultures were grown in
1184 LB medium supplemented with 100 $\mu\text{g/ml}$ ampicillin and 50 $\mu\text{g/ml}$ kanamycin at 37
1185 °C to an OD_{600nm} of 0.8 and expression was induced with 1 mM IPTG. The cells were
1186 further grown for 6 h at 37 °C, harvested and lysed in buffer C [50 mM Tris-HCl pH 8,
1187 500 mM NaCl, 1 mM MgCl₂, 10% (v/v) glycerol, 20 mM imidazole] containing 0.1
1188 mg/ml DNaseI and protease inhibitors. The lysates were cleared for 30 min at 45,000
1189 $\times g$ and incubated with 1 ml of Ni-NTA agarose (Quiagen) per 1 l of expression culture,
1190 for 2 h rotating at 4 °C. Afterwards, the matrix was transferred to a gravity-flow Econo
1191 column (49 ml volume; BioRad) and washed with buffer D [50 mM Tris-HCl pH 8.0,
1192 500 mM NaCl, 10% (v/v) glycerol, 30 mM imidazole], buffer E [50 mM Tris-HCl pH
1193 8.0, 300 mM NaCl, 10 mM imidazole, 5 mM β -mercaptoethanol], and buffer E
1194 sequentially supplemented with (i) 1 M NaCl, (ii) 10 mM MgCl₂ + 3 mM ATP, (iii) 0.5
1195 M Tris-HCl pH 7.4, or (iv) 35 mM imidazole. The BiP proteins were then eluted with
1196 buffer F [50 mM Tris-HCl pH 8.0, 300 mM NaCl, 5 mM β -mercaptoethanol, 250 mM
1197 imidazole], dialyzed against HKM (50 mM HEPES-KOH pH 7.4, 150 mM KCl, 10
1198 mM MgCl₂) and concentrated with 30 kDa MWCO centrifugal filters. The proteins
1199 were flash-frozen in aliquots and stored at -80 °C.

1200 GST-TEV-BiP constructs were purified like His₆-Smt3-FICD, above, with minor
1201 alterations. Purification proceeded without the inclusion of imidazole in the purification
1202 buffers. Cleared lysates were supplemented with 1 mM DTT and incubated with GSH-
1203 Sepharose 4B matrix (GE Healthcare) for 1 h at 4 °C. 2 CV of TNT(0.1) (25 mM Tris-

1204 HCl pH 8.0, 150 mM NaCl, 0.1 mM TCEP) was used as a final wash step before elution.
1205 GST-TEV-BiP was eluted with 10 mM HEPES-KOH pH 7.4, 20 mM Tris-HCl pH 8.0,
1206 30 mM KCl, 120 mM NaCl, 2 mM MgCl₂ and 40 mM reduced glutathione. The eluate
1207 was cleaved with TEV protease (1/200 w/w; UK 759), whilst dialysing into TN plus 1
1208 mM DTT, for 16 h at 4 °C. Uncleaved BiP was depleted by incubation, for 1 h at 4 °C,
1209 with GSH-Sepharose 4B matrix (1 ml per 5 mg of protein). The flow through was
1210 collected. Retained, cleaved material was washed from the matrix with 5 CV of
1211 TNT(0.1). All the cleaved, non-bound material was pooled. In order to AMPylate BiP,
1212 the cleaved product was combined with 1/50 (w/w) GST-TEV-FICD(45-458)^{E234G} (UK
1213 1479; purified like the GST-TEV-BiP without TEV cleavage steps). The AMPylation
1214 reaction was supplemented with 10 mM MgATP (10 mM MgCl₂ + 10 mM ATP), and
1215 incubated for 16 h at 25 °C. GST-TEV-FICD was then depleted by incubation with
1216 GSH-Sepharose 4B matrix, as above. Proteins were concentrated to > 200 μM. Aliquots
1217 were snap-frozen in liquid nitrogen and stored at -80 °C.

1218 When required, protein samples were validated as being nucleotide free (Apo) by their
1219 A_{260/280} ratio and reference to IP-RP-HPLC analysis as conducted in (Preissler *et al*,
1220 2017a).

1221 Formation of disulphide-linked FICD dimers

1222 Expression and purification of disulphide-linked dimers [of FICD^{A252C-C421S} (UK 2219)
1223 and FICD^{A252C-H363A-C421S} (trap; UK 2269)] was performed as described above with
1224 some alterations. After the affinity chromatography step, on-column cleavage was
1225 performed in TNT-Iz10 containing 1.5 μg/ml Up11-StrepII and the retained cleavage
1226 products were washed off the beads with TN-Iz10 (25 mM Tris-HCl pH 8.0, 150 mM
1227 NaCl, 10 mM imidazole) in the absence of reducing agent. The pooled eluate was
1228 concentrated and diluted 1:4 with TN-Iz10. To allow for efficient disulphide bond
1229 formation the samples were supplemented with 20 mM oxidized glutathione and
1230 incubated overnight at 4 °C. Afterwards, the protein solutions were diluted 1:2 with 25
1231 mM Tris-HCl pH 8.0 and further purified by anion-exchange and size-exclusion
1232 chromatography. The final preparations were analysed by non-reducing SDS-PAGE to
1233 confirm quantitative formation of covalently linked dimers (> 95%). Cysteine-free
1234 FICD^{C421S} (UK 2161) was purified according to the same protocol. A separate
1235 preparation of non-disulphide-bonded FICD^{A252C-C421S} (UK 2219), which was not

1236 subjected to oxidation with glutathione, was used in control experiments (Figure 3B,
1237 S3A and C).

1238 **In vitro AMPylation**

1239 Standard radioactive in vitro AMPylation reactions were performed in HKMC buffer
1240 (50 mM HEPES-KOH pH 7.4, 150 mM KCl, 10 mM MgCl₂, 1 mM CaCl₂) containing
1241 40 μM ATP, 0.034 MBq [α-³²P]-ATP (EasyTide; Perkin Elmer), 0.2 μM FICD, and 1.5
1242 μM ATP-hydrolysis and substrate-binding deficient BiP^{T229A-V461F} (UK 1825) in a final
1243 volume of 15 μl. Where indicated, samples contained 5 μM s-sFICD^{A252C-H363A-C421S}
1244 (UK 2269, trap) to sequester modified BiP. The reactions were started by addition of
1245 nucleotides. After a 20 min incubation at 25 °C the reactions were stopped by addition
1246 of 5 μl 4 × SDS sample buffer and denaturation for 5 min at 75 °C. The samples were
1247 applied to SDS-PAGE and the gels were stained with Coomassie (InstantBlue;
1248 expedeon). The dried gels were exposed to a storage phosphor screen and radioactive
1249 signals were detected with a Typhoon biomolecular imager (GE Healthcare). Signals
1250 were quantified using ImageJ64 software (NIH).

1251 The reactions to analyse AMPylation at elevated concentrations (2 or 10 μM; Figure
1252 S4A) contained 2 μM BiP^{T229A-V461F}, 80 μM ATP and 0.034 MBq [α-³²P]-ATP in a final
1253 volume of 15 μl. The reactions were stopped after 5 min incubation at 25 °C.

1254 Time course experiments (Figure 2E) were performed likewise but reactions contained
1255 40 μM ATP, 0.136 MBq [α-³²P]-ATP, 0.3 μM FICD, 2 μM BiP^{T229A-V461F}, and 5 μM
1256 trap in a final volume of 60 μl. The reactions were incubated at 30 °C and samples (15
1257 μl) were taken at different time intervals and processed as described above.

1258 To study the effect of the concentration of wild-type FICD protein on its ability to
1259 establish a pool of AMPylated BiP (Figure 3A), final reactions were setup with 400 μM
1260 ATP, 0.049 MBq [α-³²P]-ATP, 2.5 nM to 400 nM FICD (UK 2052) and 5 μM BiP^{T229A-}
1261 ^{V461F}, without or with 5 μM trap in a final volume of 15 μl. The reactions were pre-
1262 incubated for 2 h before addition of nucleotides. After 2 and 16 h incubation with
1263 nucleotides at 25 °C (as indicated) samples (5 μl) were taken and denatured by heating
1264 in SDS sample buffer for analysis.

1265 To compare the activity of disulphide-bonded FICD under non-reducing and reducing
1266 conditions (Figure 3C) s-sFICD^{A252C-C421S} protein (UK 2219) was pre-incubated 16 h at

1267 25 °C without or with 10 mM DTT and a sample was analysed by non-reducing SDS-
1268 PAGE after denaturation in SDS sample buffer containing 40 mM N-ethylmaleimide
1269 (NEM). Afterwards, AMPylation reactions (15 µl final volume) were set up with 400
1270 µM ATP, 0.049 MBq [α -³²P]-ATP, 2.5 nM to 400 nM s-sFICD^{A252C-C421S}, and 5 µM
1271 BiP^{T229A-V461F} in the presence or absence of 5 mM DTT. Samples were incubated for
1272 16 h at 25 °C and 5 µl was taken and processed for analysis by reducing SDS-PAGE as
1273 described above. Parallel reactions performed with cysteine-free FICD^{C421S} (UK 2161),
1274 which underwent the same purification and oxidation procedure, served as a control.
1275 The experiment presented in [Figure S3C](#) was performed accordingly under non-
1276 reducing conditions, but the reactions were incubated for 2 h at 25 °C and in the
1277 presence of 5 µM trap.

1278

1279 **Coupled in vitro AMPylation/deAMPylation reactions**

1280 To measure AMPylation-/deAMPylation-dependent AMP production by FICD
1281 proteins reactions were set up in HKM buffer containing 250 µM ATP, 0.0185 MBq
1282 [α -³²P]-ATP, 3 mM TCEP, 5 µM ATP-hydrolysis-deficient BiP^{T229A} (UK 838), and 2
1283 µM FICD proteins in a final volume of 30 µl. The reactions were started by addition of
1284 nucleotides and incubated for 2 h at 30 °C. Afterwards, 2 µl were spotted onto a thin
1285 layer chromatography (TLC) plate (PEI Cellulose F; Merck Millipore) pre-spotted with
1286 2 µl of nucleotide mix containing AMP, ADP, and ATP (each at 3.5 mM). The TLC
1287 plate was developed with 400 mM LiCl and 10% (v/v) acetic acid as a mobile phase
1288 and the dried plates were exposed to a storage phosphor screen. The signals were
1289 detected with a Typhoon biomolecular imager and quantified using ImageJ64.

1290

1291 **DeAMPylation measured by fluorescence polarisation (FP)**

1292 Measurement of deAMPylation kinetics was performed as described previously
1293 (Preissler *et al*, 2017a) with modifications. The probe (BiP^{V461F} modified with
1294 fluorescent, FAM-labelled AMP; BiP^{V461F}-AMP^{FAM}) was generated by pre-incubating
1295 FICD^{E234G} at 25 µM in HKM buffer with 200 µM ATP-FAM [N⁶-(6-amino)hexyl-
1296 adenosine-5'-triphosphate; Jena Bioscience] for 10 min at 30 °C, followed by addition
1297 of 25 µM His₆-tagged BiP^{V461F} (UK 182) to a final volume of 50 µl, and further
1298 incubation for 2 h at 30 °C. Afterwards, the reaction was diluted with 950 µl of HKMG-

1299 Iz20 [50 mM HEPES-KOH pH 7.4, 150 mM KCl, 10 mM MgCl₂, 5% (v/v) glycerol,
1300 20 mM imidazole] and BiP proteins were bound to 80 µl Ni-NTA agarose beads
1301 (Qiagen) for 30 min at 25 °C in the presence of 0.01% Triton X-100. Following several
1302 wash steps in the same buffer proteins were eluted in HKMG-Iz250 [50 mM HEPES-
1303 KOH pH 7.4, 150 mM KCl, 10 mM MgCl₂, 5% (v/v) glycerol, 250 mM imidazole],
1304 flash-frozen in aliquots, and stored at -80 °C.

1305 DeAMPylation reactions were performed in FP buffer [50 mM HEPES-KOH pH 7.4,
1306 150 mM KCl, 10 mM MgCl₂, 1 mM CaCl₂, 0.1% (v/v) Triton X-100] in 384-well
1307 polystyrene microplates (black, flat bottom, µCLEAR; greiner bio-one) at 30 °C in a
1308 final volume of 30 µl containing trace amounts of fluorescent BiP^{V461F}-AMP-FAM probe
1309 (17 nM) and FICD proteins (0.75 or 7.5 µM). Fluorescence polarisation of FAM ($\lambda_{\text{ex}} =$
1310 485 nm, $\lambda_{\text{em}} = 535$ nm) was measured with an Infinite F500 plate reader (Tecan). Fitting
1311 of the raw data to a single-exponential decay function was done using Prism 6.0e
1312 (GraphPad).

1313

1314 **Analytical size-exclusion chromatography**

1315 Analytical size-exclusion chromatography (SEC) was performed as described
1316 previously (Preissler *et al*, 2015a). Purified FICD proteins were adjusted to 20 µM in
1317 HKMC buffer (50 mM HEPES-KOH pH 7.4, 150 mM KCl, 10 mM MgCl₂, 1 mM
1318 CaCl₂) and incubated at 25 °C for at least 20 min before injection. From each sample
1319 10 µl was injected onto a SEC-3 HPLC column (300 Å pore size; Agilent Technologies)
1320 equilibrated with HKMC at a flow rate of 0.3 ml/min. Runs were performed at 25 °C
1321 and A_{280nm} absorbance traces were recorded. Protein standards (Bio-Rad, cat. no. 151–
1322 1901) were run as size references and the elution peaks of γ -globulin (158 kDa),
1323 ovalbumin (44 kDa), and myoglobin (17 kDa) are indicated. For dimer SEC studies
1324 in [Figure S1D-E](#), the FICD proteins were incubated for 16 h at 25 °C before injection.
1325 To investigate capture of AMPylated BiP by s-sFICD^{A252C-H363A-C421S} (UK 2269, trap),
1326 by SEC ([Figure S2H](#)), in vitro AMPylation reactions containing different combinations
1327 of 20 µM BiP^{T229A-V461F} (UK 1825), 10 µM trap, and 3 µM FICD^{L258D} (UK 2091) were
1328 performed in HKMC (supplemented with 2 mM ATP when indicated) and incubated
1329 for 1.5 h at 30 °C before injection.

1330

1331 **Fluorescence detection system sedimentation velocity analytical**
1332 **ultracentrifugation (FDS-SV-AUC)**

1333 Bacterial expression and purification of FICD proteins carrying an N-terminal cysteine
1334 for site-specific labelling (FICD^{NC}, UK 2339, and FICD^{L258D-NC}, UK 2367) was
1335 performed as described above with the following alterations: Cells were lysed in the
1336 presence of 5 mM β -mercaptoethanol and the eluate pool after affinity chromatography
1337 and on-column cleavage was supplemented with 5 mM DTT and diluted 1:2 with 25
1338 mM Tris-HCl pH 8.0 containing 0.2 mM TCEP. The subsequent anion-exchange
1339 chromatography step was performed with buffer solutions AEX-A and AEX-B
1340 supplemented with 0.2 mM TCEP. Afterwards, the peak fractions corresponding to the
1341 dimeric form of FICD were pooled and concentrated. The protein at 200 μ M was
1342 labelled in 150 μ l with 600 μ M Oregon Green 488-iodoacetamide in the presence of
1343 0.5 mM TCEP and 0.1 mM EDTA for 16 h at 4 °C. The reaction was quenched with 2
1344 mM DTT for 10 min at 25 °C. Afterwards the sample was passed through a CentriPure
1345 P2 desalting column (emp) equilibrated in SEC buffer containing 0.2 mM TCEP. The
1346 eluate was applied to size-exclusion chromatography using a Superdex 200 10/300 GL
1347 column (GE Healthcare) in the presence of 0.2 mM TCEP. The fractions of the A_{280nm}
1348 peak, corresponding to dimeric FICD, were pooled and the concentration of TCEP was
1349 adjusted to 1 mM. The proteins were concentrated and frozen in aliquots. The protein
1350 concentration was determined after denaturing the proteins with 6 M guanidine
1351 hydrochloride by measuring absorbance at 280 nm and 496 nm with a NanoDrop
1352 Spectrophotometer (Thermo Fisher Scientific). The concentration was calculated using
1353 the following equation:

1354 Protein concentration (M) = $[A_{280nm} - (A_{496nm} \times 0.12)]/\epsilon$

1355 Where 0.12 is the correction factor for the fluorophore's absorbance at 280 nm, and ϵ
1356 is the calculated molar extinction coefficient of FICD (29,340 cm⁻¹M⁻¹). The labelling
1357 efficiency of the FICD^{NC} preparation was 74% as calculated based on the A_{496nm} value
1358 and assuming an extinction coefficient for Oregon Green 488 of 70,000 cm⁻¹M⁻¹. The
1359 labelling efficiency of the monomeric FICD^{L258D-NC} control preparation was 9.6%.
1360 Labelling of the endogenous cysteine residue (Cys421) of wild-type FICD was very
1361 inefficient (< 1%) and thus considered negligible.

1362 Samples of Oregon Green-labelled FICD in 50 mM HEPES-KOH pH 7.4, 150 mM
1363 KCl, 10 mM MgCl₂, 1 mM CaCl₂, 0.3 mM TCEP, 0.1 % Tween-20, 0.15 mg/ml BSA
1364 (Sigma), ranging in concentration from 1.6 μM to 31 pM, were centrifuged at 45,000
1365 rpm at 20 °C in an An50Ti rotor using an Optima XL-I analytical ultracentrifuge
1366 (Beckmann) equipped with a fluorescence optical detection system (Aviv Biomedical)
1367 with fixed excitation at 488 nm and fluorescence detection at > 505 nm. Data were
1368 processed and analysed using SEDFIT 15 and SEDPHAT 13b (Schuck, 2003)
1369 according to the published protocol for high-affinity interactions detected by
1370 fluorescence (Chaturvedi *et al*, 2017). Data were plotted with Prism 6.0e (GraphPad)
1371 or GUSI (Brautigam, 2015).

1372

1373 **Differential Scanning Fluorimetry (DSF)**

1374 DSF experiments were performed on an ABI 7500 qPCR machine (Applied
1375 Biosciences). Experiments were carried out in 96-well qPCR plates (Thermofisher),
1376 with each sample in technical triplicate and in a final volume of 20 μl. Protein was used
1377 at a final concentration of 2 μM, ligands at the concentration indicated in the figure
1378 legend (2.5-20 mM), and SYPRO Orange (Thermofisher) dye at a 10x concentration in
1379 a buffer of HKM plus 1 mM TCEP (unless otherwise specified). For the ATP titration
1380 (Figure 4F and S4E), the DSF buffer was supplemented with an additional 15 mM
1381 MgCl₂ (25 mM total MgCl₂). Fluorescence of the SYPRO Orange dye was monitored
1382 over a temperature range of 20-95 °C using the VIC filter set. Data was then analysed
1383 in Prism 7.0e (GraphPad), with melting temperature calculated as the global minimums
1384 of the negative first derivatives of the relative fluorescent unit melt curves (with respect
1385 to temperature).

1386

1387 **Bio-layer interferometry (BLI)**

1388 In vitro biotinylation

1389 Ligands for BLI were generated from the tag cleaved forms of unmodified or
1390 AMPylated GST-TEV-AviTag-haBiPV461F(19-654) (UK 2043) and GST-TEV-
1391 AviTag-haBiP(28-635)^{T229A-V461F} (UK 2331). Biotinylation was conducted in vitro on
1392 100 μM target protein, with 200 μM biotin (Sigma), 2 μM GST-BirA (UK 1801) in a
1393 buffer of 2 mM ATP, 5 mM MgCl₂, 25 mM Tris-HCl pH 8.0, 150 mM NaCl and 1

1394 mM TCEP. The reaction mixture was incubated for 16 h at 4 °C. Excess biotin was
1395 removed by size-exclusion chromatography on a S200 10/300 GL column (GE
1396 Healthcare) with a distal 1 ml GStrap 4B (GE Healthcare), connected in series. The
1397 ligand was confirmed as being > 95% biotinylated as judged by streptavidin gel-shift.
1398 In the case of Biotinylated-AviTag-haBiP(28-635)^{T229A-V461F} this protein was also
1399 made nucleotide free by the addition of 2 U CIP (NEB) per mg of BiP, plus extensive
1400 dialysis into TN buffer with 1 mM DTT and 2 mM EDTA (dialysed with several
1401 dialysate changes, for 2 days at 4 °C). The protein was then purified by anion
1402 exchange chromatography on a MonoQ 5/50 GL column (GE Healthcare) using
1403 buffers AEX-A and AEX-B with a gradient of 7.5-50% B over 20 CV at a flow rate
1404 of 1 ml/min. The protein was concentrated using a 30 kDa MWCO centrifugal filters
1405 (Amicon Ultra; Merck Millipore) and then gel filtered, as above, but into an HKM
1406 buffer. Fractions were pooled and supplemented with 1 mM TCEP. All proteins after
1407 biotinylation and purification were concentrated to > 20 µM, flash-frozen in small
1408 aliquots and stored at -80 °C.

1409 Kinetic experiments

1410 All BLI experiments were conducted on the FortéBio Octet RED96 System (Pall
1411 FortéBio) in a buffer basis of HKM plus 0.05% Triton X-100 (HKMTx). Nucleotide
1412 was added as indicated. Streptavidin (SA)-coated biosensors (Pall FortéBio) were
1413 hydrated in HKMTx for at least 30 min prior to use. All BLI experiments were
1414 conducted at 30 °C with the experimental steps as indicated in the text. BLI reactions
1415 were prepared in 200 µl volumes in 96 well microplates (greiner bio-one, cat. no.
1416 655209). Ligand loading was performed for 300 to 600 s at a shake speed of 1000
1417 rpm until a binding signal of 1 nm was reached. The immobilised ligand sensor was
1418 then baselined in assay solution for at least 200 s. For kinetic experiments with
1419 biotinylated-AviTag-haBiP(28-635)^{T229A-V461F}:Apo [BiP^{T229A-V461F}:Apo (UK 2331)]
1420 loaded on the tip, a 10 Hz acquisition rate was used and the baseline, association and
1421 dissociation steps were conducted at a 400 rpm shake speed. Preceding the baseline
1422 step biotinylated BiP^{T229A-V461F}:Apo was also activated with or without ATP (2 mM
1423 unless otherwise stated), as indicated, for 300 s at a 1000 rpm shake speed. In these
1424 experiments FICD analyte association or dissociation steps were conducted in the
1425 presence or absence of nucleotide, as indicated, with ATP at 8 mM and ADP at 2
1426 mM. These concentrations were chosen in an attempt to saturate either monomeric or

1427 dimeric FICD with the respective nucleotide [K_d of MgADP for wild-type FICD is
1428 1.52 μ M by ITC (Bunney *et al*, 2014); $K_{1/2}$ of ATP induced FICD T_m shift in the low
1429 mM range] and/or to make ATP binding non-rate limiting. In [Figure S8A](#), as a control
1430 for the absence of substantial ATP dissociation from BiP, between the activation and
1431 baseline step an additional 1500 s BiP wash (\pm ATP) was included, as indicated.
1432 Other BLI experiments were conducted with all steps at a 1000 rpm shake speed with
1433 a 5 Hz acquisition rate. All association-dissociation kinetics were completed in \leq
1434 1500 s. Data was processed in Prism 7.0e (GraphPad). Note, the FICD variants used
1435 as analytes in all BLI experiments were catalytically inactive His363Ala variants
1436 (used at 250 nM).

1437 In the dimer dissociation BLI experiments biotinylated AviTag-FICD(104-458)^{H363A}
1438 (UK 2422) was diluted to 3 nM and incubated for 10 min at 25 °C with either dimeric
1439 FICD^{H363A} or monomeric FICD^{L258D-H363A} (at 300 nM) in HKMTx. After this
1440 incubation period the streptavidin biosensors were loaded until those immobilising
1441 hetero-labelled dimers (biotinylated AviTag-FICD(104-458)^{H363A} with FICD^{H363A})
1442 were loaded to a 1 nm displacement. Dissociation was initiated by dipping in HKTx
1443 buffer (50 mM HEPES-KOH pH 7.4, 150 mM KCl and 0.05% Triton X-100) \pm
1444 nucleotide at 5 mM, as indicated. Data was processed by subtracting the respective
1445 monomer incubated biotinylated FICD tip from the dimeric hetero-labelled dimer
1446 dissociation, followed by fitting of the corrected dissociation to mono-exponential
1447 decay using Prism 7.0e (GraphPad).

1448

1449 **Protein crystallization and structure determination**

1450 FICD proteins were purified as above in *Protein Purification* but gel filtered into a
1451 final buffer of 10 mM Tris-HCl pH 8.0, 150 mM NaCl and 1 mM TCEP [T(10)NT].
1452 Proteins were diluted to 9 mg/ml in T(10)NT prior to crystallisation, via sitting drop
1453 vapour diffusion. For structures containing ATP, final diluted protein solutions were
1454 supplemented with MgATP (from a pH 7.4, 100 mM stock solution) to a final
1455 concentration of 10 mM. A drop ratio of protein solution to crystallisation well
1456 solution of 200:100 nl was used. Where applicable crystals were obtained by
1457 microseeding (D'Arcy *et al*, 2007), from conditions provided in [Table S1](#). In these
1458 instances, a drop ratio of protein solution to water-diluted seeds to crystallisation well

1459 solution of 150:50:100 nl was used. The best diffracting crystals were obtained in
1460 crystallisation conditions detailed in [Table S1](#).

1461 Diffraction data were collected from the Diamond Light Source, and the data
1462 processed using XDS (Kabsch, 2010) and the CCP4 module Aimless (Winn *et al*,
1463 2011; Evans & Murshudov, 2013). Structures were solved by molecular replacement
1464 using the CCP4 module Phaser (McCoy *et al*, 2007; Winn *et al*, 2011). For the
1465 FICD^{L258D}:Apo and FICD:ATP structures the human FICD protein (FICD:MgADP)
1466 structure 4U0U from the Protein Data Bank (PDB) was used as a search model.
1467 Subsequent molecular replacements used the solved FICD^{L258D}:Apo structure as a
1468 search model. Manual model building was carried out in COOT (Emsley *et al*, 2010)
1469 and refined using re mac5 (Winn *et al*, 2003). Metal binding sites were validated
1470 using the CheckMyMetal server (Zheng *et al*, 2017). Polder (OMIT) maps were
1471 generated by using the Polder Map module of Phenix (Liebschner *et al*, 2017; Adams
1472 *et al*, 2010). Structural figures were prepared using UCSF Chimera (Pettersen *et al*,
1473 2004) and PyMol (Schrödinger, LLC, 2015).

1474 **References**

- 1475 Adams PD, Afonine P V, Bunkóczi G, Chen VB, Davis IW, Echols N, Headd JJ,
1476 Hung L-W, Kapral GJ, Grosse-Kunstleve RW, McCoy AJ, Moriarty NW,
1477 Oeffner R, Read RJ, Richardson DC, Richardson JS, Terwilliger TC & Zwart PH
1478 (2010) PHENIX: a comprehensive Python-based system for macromolecular
1479 structure solution. *Acta Crystallogr. D. Biol. Crystallogr.* **66**: 213–21 Available
1480 at: <http://scripts.iucr.org/cgi-bin/paper?S0907444909052925> [Accessed August
1481 11, 2017]
- 1482 Andrews LD, Fenn TD & Herschlag D (2013) Ground State Destabilization by
1483 Anionic Nucleophiles Contributes to the Activity of Phosphoryl Transfer
1484 Enzymes. *PLoS Biol.* **11**: e1001599 Available at:
1485 <http://dx.plos.org/10.1371/journal.pbio.1001599> [Accessed August 30, 2018]
- 1486 Avezov E, Cross BCS, Kaminski Schierle GS, Winters M, Harding HP, Melo EP,
1487 Kaminski CF & Ron D (2013) Lifetime imaging of a fluorescent protein sensor
1488 reveals surprising stability of ER thiol redox. *J. Cell Biol.* **201**: 337–49 Available
1489 at: <http://www.jcb.org/lookup/doi/10.1083/jcb.201211155> [Accessed September
1490 20, 2018]
- 1491 Brautigam CA (2015) Calculations and Publication-Quality Illustrations for
1492 Analytical Ultracentrifugation Data. *Methods Enzymol.* **562**: 109–33 Available
1493 at: <http://linkinghub.elsevier.com/retrieve/pii/S0076687915002992> [Accessed
1494 September 20, 2018]
- 1495 Broncel M, Serwa RA, Bunney TD, Katan M & Tate EW (2016) Global Profiling of
1496 Huntingtin-associated protein E (HYPE)-Mediated AMPylation through a
1497 Chemical Proteomic Approach. *Mol. Cell. Proteomics* **15**: 715–725 Available at:
1498 <http://www.mcponline.org/lookup/doi/10.1074/mcp.O115.054429> [Accessed
1499 September 3, 2016]
- 1500 Bunney TD, Cole AR, Broncel M, Esposito D, Tate EW & Katan M (2014) Crystal
1501 structure of the human, FIC-domain containing protein HYPE and implications
1502 for its functions. *Structure* **22**: 1831–43 Available at:
1503 <http://www.cell.com/article/S0969212614003347/fulltext> [Accessed February
1504 14, 2016]

- 1505 Casey AK, Moehlman AT, Zhang J, Servage KA, Krämer H & Orth K (2017) Fic-
1506 mediated deAMPylation is not dependent on homo-dimerization and rescues
1507 toxic AMPylation in flies. *J. Biol. Chem.*: jbc.M117.799296 Available at:
1508 <http://www.ncbi.nlm.nih.gov/pubmed/29089387> [Accessed November 2, 2017]
- 1509 Chambers JE, Petrova K, Tomba G, Vendruscolo M & Ron D (2012) ADP
1510 ribosylation adapts an ER chaperone response to short-term fluctuations in
1511 unfolded protein load. *J. Cell Biol.* **198**: 371–85 Available at:
1512 <http://jcb.rupress.org/content/198/3/371> [Accessed March 31, 2016]
- 1513 Chaturvedi SK, Ma J, Zhao H & Schuck P (2017) Use of fluorescence-detected
1514 sedimentation velocity to study high-affinity protein interactions. *Nat. Protoc.*
1515 **12**: 1777–1791 Available at:
1516 <http://www.nature.com/doifinder/10.1038/nprot.2017.064> [Accessed September
1517 20, 2018]
- 1518 D’Arcy A, Villard F & Marsh M (2007) An automated microseed matrix-screening
1519 method for protein crystallization. *Acta Crystallogr. Sect. D Biol. Crystallogr.*
1520 **63**: 550–554 Available at: [http://scripts.iucr.org/cgi-](http://scripts.iucr.org/cgi-bin/paper?S0907444907007652)
1521 [bin/paper?S0907444907007652](http://scripts.iucr.org/cgi-bin/paper?S0907444907007652) [Accessed September 14, 2018]
- 1522 Dedic E, Alsarraf H, Welner DH, Østergaard O, Klychnikov OI, Hensbergen PJ,
1523 Corver J, van Leeuwen HC & Jørgensen R (2016) A Novel Fic (Filamentation
1524 Induced by cAMP) Protein from *Clostridium difficile* Reveals an Inhibitory
1525 Motif-independent Adenylylation/AMPylation Mechanism. *J. Biol. Chem.* **291**:
1526 13286–300 Available at: <http://www.ncbi.nlm.nih.gov/pubmed/27076635>
1527 [Accessed August 2, 2017]
- 1528 Dey M, Cao C, Sicheri F & Dever TE (2007) Conserved Intermolecular Salt Bridge
1529 Required for Activation of Protein Kinases PKR, GCN2, and PERK. *J. Biol.*
1530 *Chem.* **282**: 6653–6660 Available at:
1531 <http://www.ncbi.nlm.nih.gov/pubmed/17202131> [Accessed September 18, 2018]
- 1532 Emsley P, Lohkamp B, Scott WG & Cowtan K (2010) Features and development of
1533 *Coot*. *Acta Crystallogr. Sect. D Biol. Crystallogr.* **66**: 486–501 Available at:
1534 <http://www.ncbi.nlm.nih.gov/pubmed/20383002> [Accessed August 11, 2017]
- 1535 Engel P, Goepfert A, Stanger F V, Harms A, Schmidt A, Schirmer T & Dehio C
1536 (2012) Adenylylation control by intra- or intermolecular active-site obstruction

- 1537 in Fic proteins. *Nature* **482**: 107–10 Available at:
1538 <http://dx.doi.org/10.1038/nature10729> [Accessed February 8, 2016]
- 1539 Evans PR & Murshudov GN (2013) How good are my data and what is the
1540 resolution? *Acta Crystallogr. D. Biol. Crystallogr.* **69**: 1204–14 Available at:
1541 <http://www.ncbi.nlm.nih.gov/pubmed/23793146> [Accessed March 11, 2019]
- 1542 Garcia-Pino A, Christensen-Dalsgaard M, Wyns L, Yarmolinsky M, Magnuson RD,
1543 Gerdes K & Loris R (2008) Doc of prophage P1 is inhibited by its antitoxin
1544 partner Phd through fold complementation. *J. Biol. Chem.* **283**: 30821–7
1545 Available at: <http://www.ncbi.nlm.nih.gov/pubmed/18757857> [Accessed
1546 September 1, 2018]
- 1547 Goepfert A, Stanger F V., Dehio C & Schirmer T (2013) Conserved Inhibitory
1548 Mechanism and Competent ATP Binding Mode for Adenylyltransferases with
1549 Fic Fold. *PLoS One* **8**: e64901 Available at:
1550 <http://dx.plos.org/10.1371/journal.pone.0064901> [Accessed August 10, 2017]
- 1551 Ham H, Woolery AR, Tracy C, Stenesen D, Krämer H & Orth K (2014) Unfolded
1552 protein response-regulated Drosophila Fic (dFic) protein reversibly AMPylates
1553 BiP chaperone during endoplasmic reticulum homeostasis. *J. Biol. Chem.* **289**:
1554 36059–69 Available at: <http://www.jbc.org/content/289/52/36059> [Accessed
1555 March 31, 2016]
- 1556 Kabsch W (2010) XDS. *Acta Crystallogr. D. Biol. Crystallogr.* **66**: 125–32 Available
1557 at: <http://www.ncbi.nlm.nih.gov/pubmed/20124692> [Accessed August 11, 2017]
- 1558 Khater S & Mohanty D (2015a) In silico identification of AMPylating enzymes and
1559 study of their divergent evolution. *Sci. Rep.* **5**: 10804 Available at:
1560 <http://www.nature.com/srep/2015/150603/srep10804/full/srep10804.html>
1561 [Accessed February 11, 2016]
- 1562 Khater S & Mohanty D (2015b) Deciphering the Molecular Basis of Functional
1563 Divergence in AMPylating Enzymes by Molecular Dynamics Simulations and
1564 Structure Guided Phylogeny. *Biochemistry* **54**: 5209–24 Available at:
1565 <http://dx.doi.org/10.1021/acs.biochem.5b00351> [Accessed February 14, 2016]
- 1566 Laitusis AL, Brostrom MA & Brostrom CO (1999) The dynamic role of GRP78/BiP
1567 in the coordination of mRNA translation with protein processing. *J. Biol. Chem.*

- 1568 **274:** 486–93 Available at: <http://www.ncbi.nlm.nih.gov/pubmed/9867869>
1569 [Accessed September 13, 2018]
- 1570 Lee KPK, Dey M, Neculai D, Cao C, Dever TE & Sicheri F (2008) Structure of the
1571 dual enzyme Ire1 reveals the basis for catalysis and regulation in
1572 nonconventional RNA splicing. *Cell* **132:** 89–100 Available at:
1573 <http://linkinghub.elsevier.com/retrieve/pii/S009286740701478X> [Accessed
1574 September 18, 2018]
- 1575 Liebschner D, Afonine P V., Moriarty NW, Poon BK, Sobolev O V., Terwilliger TC
1576 & Adams PD (2017) Polder maps: improving OMIT maps by excluding bulk
1577 solvent. *Acta Crystallogr. Sect. D Struct. Biol.* **73:** 148–157 Available at:
1578 <http://www.ncbi.nlm.nih.gov/pubmed/28177311> [Accessed August 28, 2018]
- 1579 McCoy AJ, Grosse-Kunstleve RW, Adams PD, Winn MD, Storoni LC & Read RJ
1580 (2007) Phaser crystallographic software. *J. Appl. Crystallogr.* **40:** 658–674
1581 Available at: <http://www.ncbi.nlm.nih.gov/pubmed/19461840> [Accessed August
1582 11, 2017]
- 1583 Moehlman AT, Casey AK, Servage K, Orth K & Krämer H (2018) Adaptation to
1584 constant light requires Fic-mediated AMPylation of BiP to protect against
1585 reversible photoreceptor degeneration. *Elife* **7:** Available at:
1586 <https://elifesciences.org/articles/38752> [Accessed August 23, 2018]
- 1587 Pettersen EF, Goddard TD, Huang CC, Couch GS, Greenblatt DM, Meng EC &
1588 Ferrin TE (2004) UCSF Chimera - A visualization system for exploratory
1589 research and analysis. *J. Comput. Chem.* **25:** 1605–1612 Available at:
1590 <http://www.ncbi.nlm.nih.gov/pubmed/15264254> [Accessed August 28, 2018]
- 1591 Preissler S, Chambers JE, Crespillo-Casado A, Avezov E, Miranda E, Perez J,
1592 Hendershot LM, Harding HP & Ron D (2015a) Physiological modulation of BiP
1593 activity by trans-protomer engagement of the interdomain linker. *Elife* **4:** e08961
1594 Available at: <http://elifesciences.org/content/4/e08961v1> [Accessed March 31,
1595 2016]
- 1596 Preissler S, Rato C, Chen R, Antrobus R, Ding S, Fearnley IM & Ron D (2015b)
1597 AMPylation matches BiP activity to client protein load in the endoplasmic
1598 reticulum. *Elife* **4:** e12621 Available at:
1599 <http://elifesciences.org/content/4/e12621.abstract> [Accessed January 7, 2016]

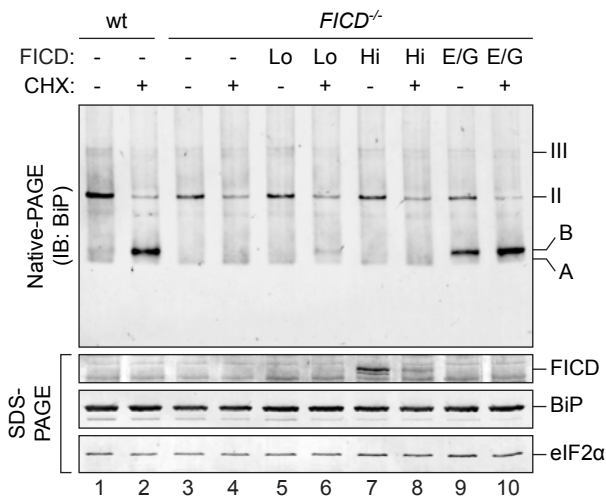
- 1600 Preissler S, Rato C, Perera L, Saudek V & Ron D (2017a) FICD acts bifunctionally to
1601 AMPylate and de-AMPylate the endoplasmic reticulum chaperone BiP. *Nat.*
1602 *Struct. Mol. Biol.* **24**: 23–29 Available at:
1603 <http://www.ncbi.nlm.nih.gov/pubmed/27918543> [Accessed January 2, 2017]
- 1604 Preissler S, Rohland L, Yan Y, Chen R, Read RJ & Ron D (2017b) AMPylation
1605 targets the rate-limiting step of BiP's ATPase cycle for its functional
1606 inactivation. *Elife* **6**: e29428 Available at: <https://elifesciences.org/articles/29428>
1607 [Accessed April 4, 2018]
- 1608 Rahman M, Ham H, Liu X, Sugiura Y, Orth K & Krämer H (2012) Visual
1609 neurotransmission in *Drosophila* requires expression of Fic in glial capitate
1610 projections. *Nat. Neurosci.* **15**: 871–875 Available at:
1611 <http://www.nature.com/articles/nn.3102> [Accessed August 23, 2018]
- 1612 Ruben EA, Schwans JP, Sonnett M, Natarajan A, Gonzalez A, Tsai Y & Herschlag D
1613 (2013) Ground state destabilization from a positioned general base in the
1614 Ketosteroid isomerase active site. *Biochemistry* **52**: 1074–1081 Available at:
1615 <http://www.ncbi.nlm.nih.gov/pubmed/23311398> [Accessed August 30, 2018]
- 1616 Sanyal A, Chen AJ, Nakayasu ES, Lazar CS, Zbornik EA, Worby CA, Koller A &
1617 Mattoo S (2015) A Novel Link between Fic (Filamentation Induced by cAMP)-
1618 mediated Adenylation/AMPylation and the Unfolded Protein Response. *J.*
1619 *Biol. Chem.* **290**: 8482–8499 Available at:
1620 <http://www.jbc.org/lookup/doi/10.1074/jbc.M114.618348> [Accessed September
1621 3, 2016]
- 1622 Schrödinger, LLC (2015) The {PyMOL} Molecular Graphics System, Version~1.8
- 1623 Schuck P (2003) On the analysis of protein self-association by sedimentation velocity
1624 analytical ultracentrifugation. *Anal. Biochem.* **320**: 104–24 Available at:
1625 <http://www.ncbi.nlm.nih.gov/pubmed/12895474> [Accessed September 20, 2018]
- 1626 Scorsone KA, Panniers R, Rowlands AG & Henshaw EC (1987) Phosphorylation of
1627 eukaryotic initiation factor 2 during physiological stresses which affect protein
1628 synthesis. *J. Biol. Chem.* **262**: 14538–43 Available at:
1629 <http://www.ncbi.nlm.nih.gov/pubmed/3667588> [Accessed September 20, 2018]
- 1630 Sekine Y, Zyryanova A, Crespillo-Casado A, Amin-Wetzel N, Harding HP & Ron D

- 1631 (2016) Paradoxical Sensitivity to an Integrated Stress Response Blocking
1632 Mutation in Vanishing White Matter Cells. *PLoS One* **11**: e0166278 Available
1633 at: <http://dx.plos.org/10.1371/journal.pone.0166278> [Accessed September 20,
1634 2018]
- 1635 Stanger F V, Burmann BM, Harms A, Aragão H, Mazur A, Sharpe T, Dehio C, Hiller
1636 S & Schirmer T (2016) Intrinsic regulation of FIC-domain AMP-transferases by
1637 oligomerization and automodification. *Proc. Natl. Acad. Sci. U. S. A.* **113**: E529-
1638 37 Available at: <http://www.pnas.org/content/113/5/E529.long> [Accessed April
1639 18, 2016]
- 1640 Truttmann MC, Cruz VE, Guo X, Engert C, Schwartz TU & Ploegh HL (2016) The
1641 *Caenorhabditis elegans* Protein FIC-1 Is an AMPylase That Covalently Modifies
1642 Heat-Shock 70 Family Proteins, Translation Elongation Factors and Histones.
1643 *PLoS Genet.* **12**: e1006023 Available at:
1644 <http://dx.plos.org/10.1371/journal.pgen.1006023> [Accessed September 3, 2016]
- 1645 Veyron S, Oliva G, Rolando M, Buchrieser C, Peyroche G & Cherfils J (2019) A
1646 Ca²⁺-regulated deAMPylation switch in human and bacterial FIC proteins. *Nat.*
1647 *Commun.* **10**: 1142 Available at: [http://www.nature.com/articles/s41467-019-](http://www.nature.com/articles/s41467-019-09023-1)
1648 09023-1 [Accessed March 11, 2019]
- 1649 Walter P & Ron D (2011) The unfolded protein response: from stress pathway to
1650 homeostatic regulation. *Science* **334**: 1081–6 Available at:
1651 <http://science.sciencemag.org/content/334/6059/1081.abstract> [Accessed March
1652 8, 2015]
- 1653 Wieteska L, Shahidi S & Zhuravleva A (2017) Allosteric fine-tuning of the
1654 conformational equilibrium poises the chaperone BiP for post-translational
1655 regulation. *Elife* **6**: e29430 Available at: <https://elifesciences.org/articles/29430>
1656 [Accessed October 24, 2017]
- 1657 Winn MD, Ballard CC, Cowtan KD, Dodson EJ, Emsley P, Evans PR, Keegan RM,
1658 Krissinel EB, Leslie AGW, McCoy A, McNicholas SJ, Murshudov GN, Pannu
1659 NS, Potterton EA, Powell HR, Read RJ, Vagin A & Wilson KS (2011) Overview
1660 of the CCP4 suite and current developments. *Acta Crystallogr. D. Biol.*
1661 *Crystallogr.* **67**: 235–42 Available at: [http://scripts.iucr.org/cgi-](http://scripts.iucr.org/cgi-bin/paper?S0907444910045749)
1662 bin/paper?S0907444910045749 [Accessed August 11, 2017]

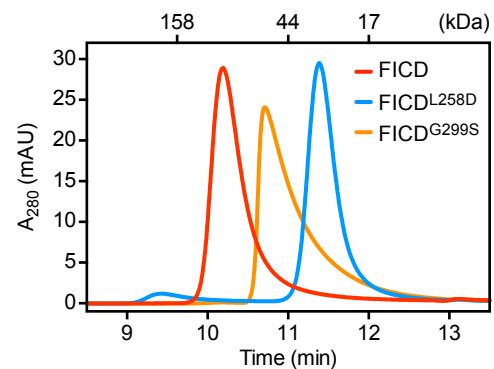
- 1663 Winn MD, Murshudov GN & Papiz MZ (2003) Macromolecular TLS Refinement in
1664 REFMAC at Moderate Resolutions. *Methods Enzymol.* **374**: 300–321 Available
1665 at:
1666 [https://www.sciencedirect.com/science/article/pii/S0076687903740142?via%3Di](https://www.sciencedirect.com/science/article/pii/S0076687903740142?via%3Dihub)
1667 [hub](https://www.sciencedirect.com/science/article/pii/S0076687903740142?via%3Dihub) [Accessed August 28, 2018]
- 1668 Worby CA, Mattoo S, Kruger RP, Corbeil LB, Koller A, Mendez JC, Zekarias B,
1669 Lazar C & Dixon JE (2009) The fic domain: regulation of cell signaling by
1670 adenylylation. *Mol. Cell* **34**: 93–103 Available at:
1671 <http://www.cell.com/article/S1097276509001981/fulltext> [Accessed April 1,
1672 2016]
- 1673 Xiao J, Worby CA, Mattoo S, Sankaran B & Dixon JE (2010) Structural basis of Fic-
1674 mediated adenylylation. *Nat. Struct. Mol. Biol.* **17**: 1004–10 Available at:
1675 <http://dx.doi.org/10.1038/nsmb.1867> [Accessed February 8, 2016]
- 1676 Zheng H, Cooper DR, Porebski PJ, Shabalin IG, Handing KB & Minor W (2017)
1677 *CheckMyMetal* : a macromolecular metal-binding validation tool. *Acta*
1678 *Crystallogr. Sect. D Struct. Biol.* **73**: 223–233 Available at:
1679 <http://scripts.iucr.org/cgi-bin/paper?S2059798317001061> [Accessed August 31,
1680 2018]
- 1681
1682
1683
1684

Figure 1

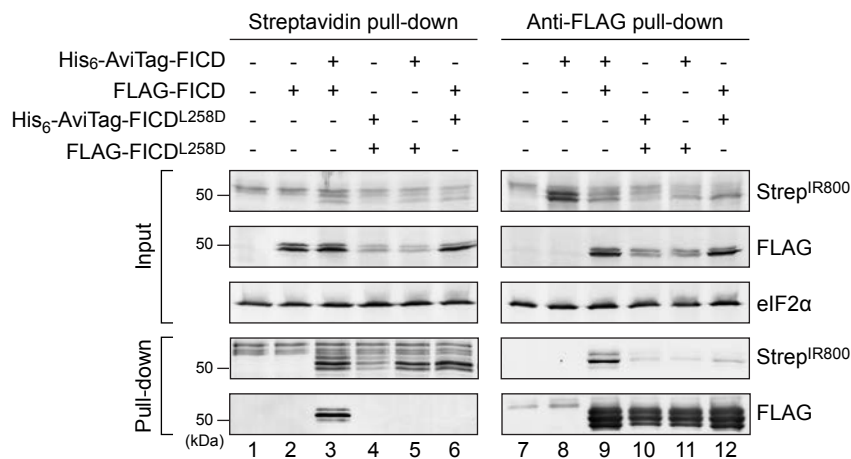
A



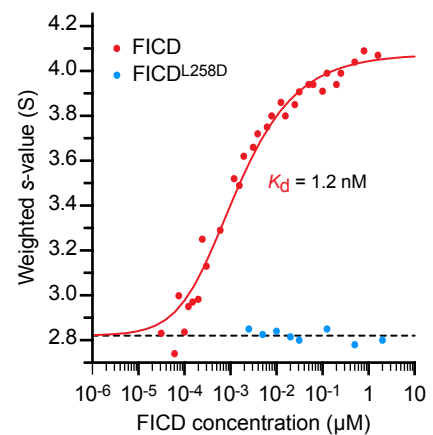
D



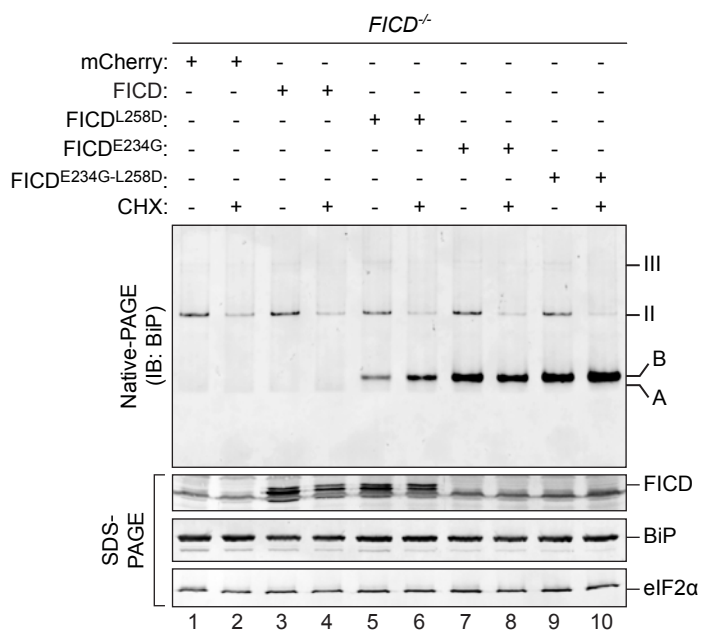
B



E



C



F

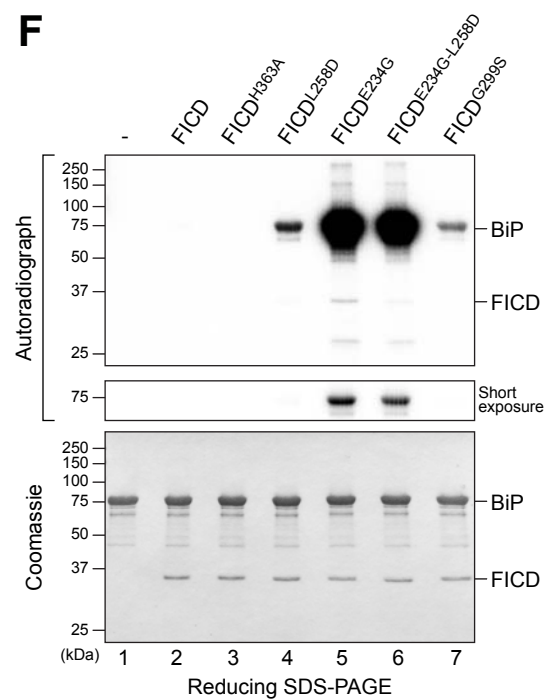


Figure 2

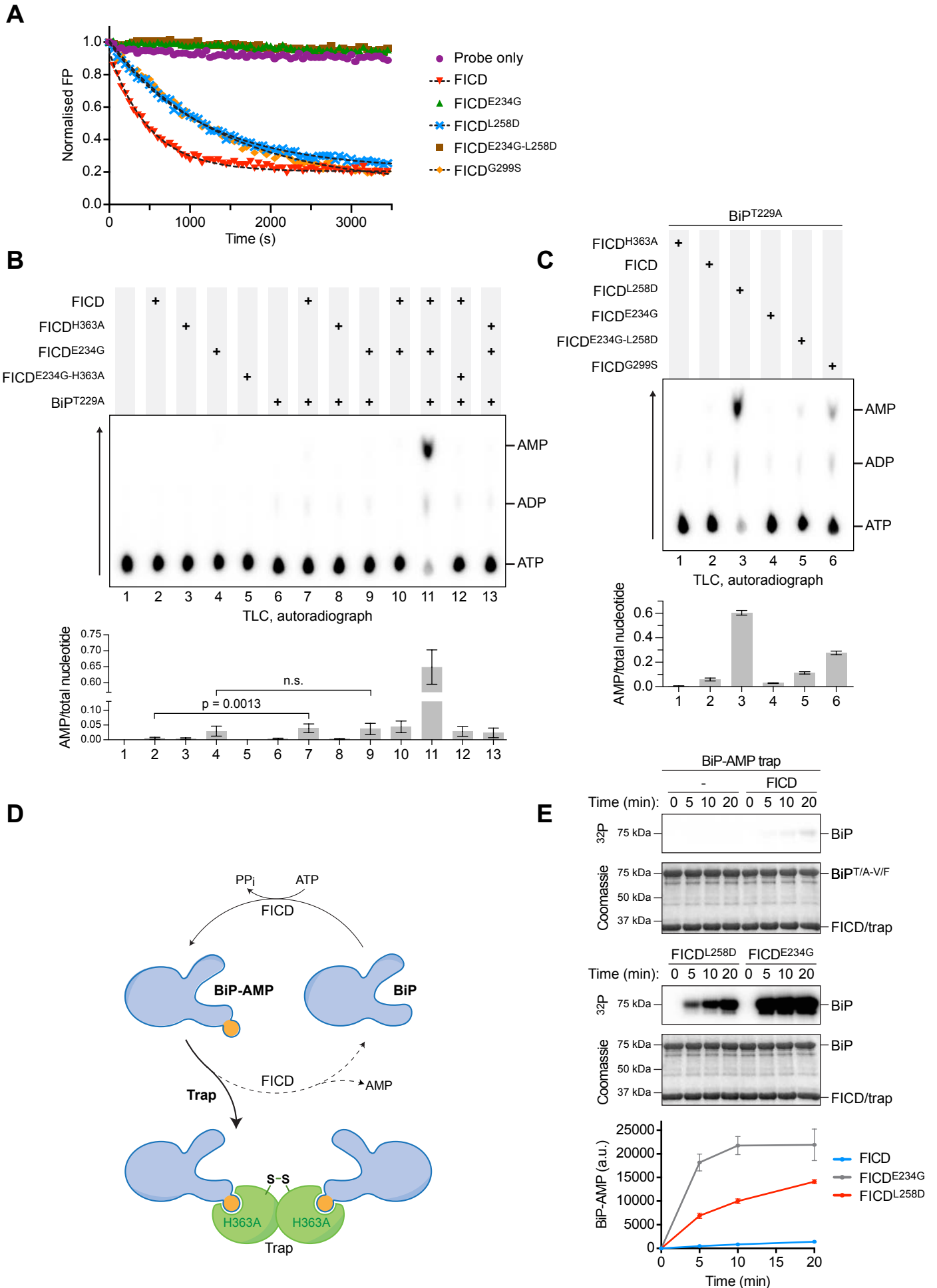


Figure 3

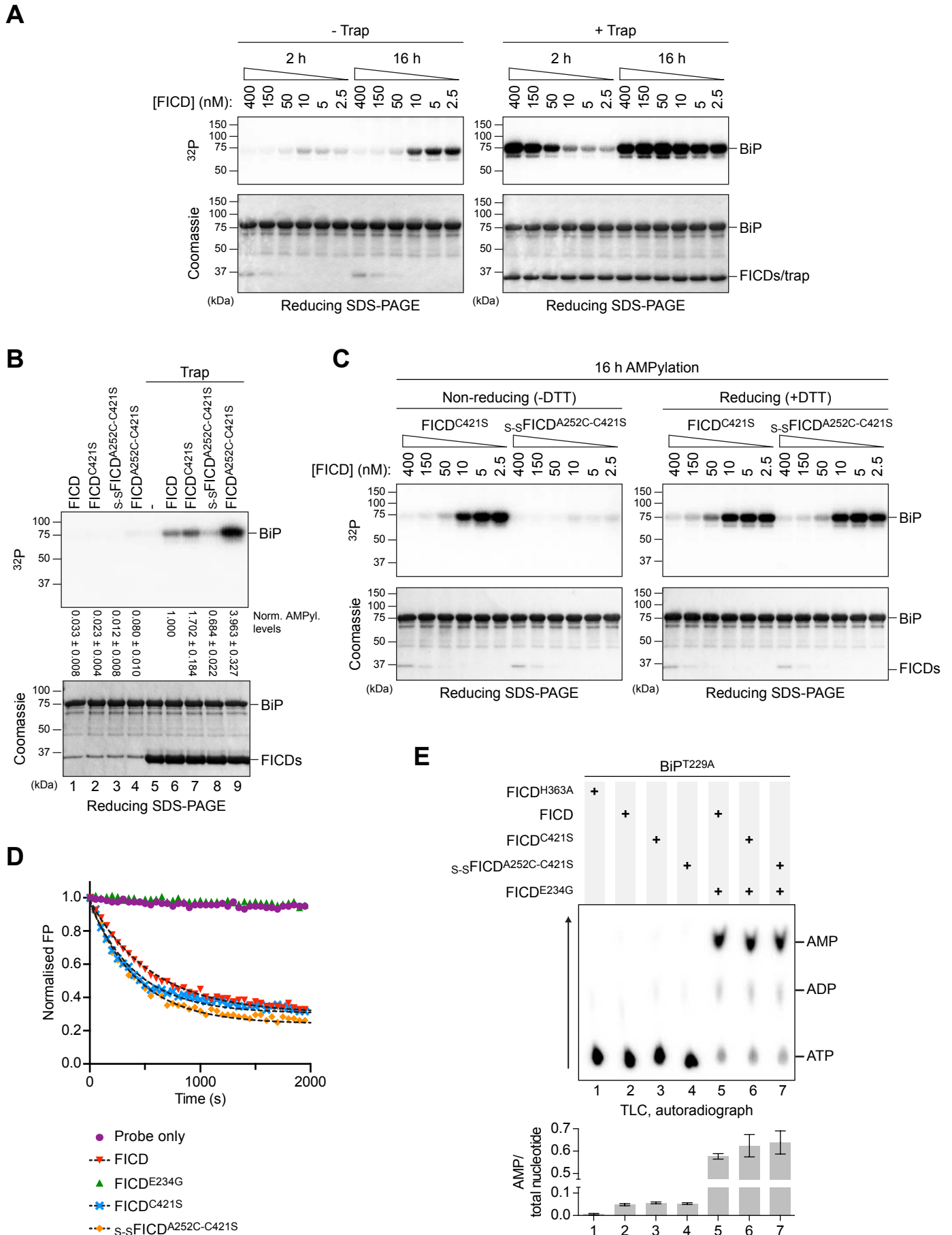


Figure 4

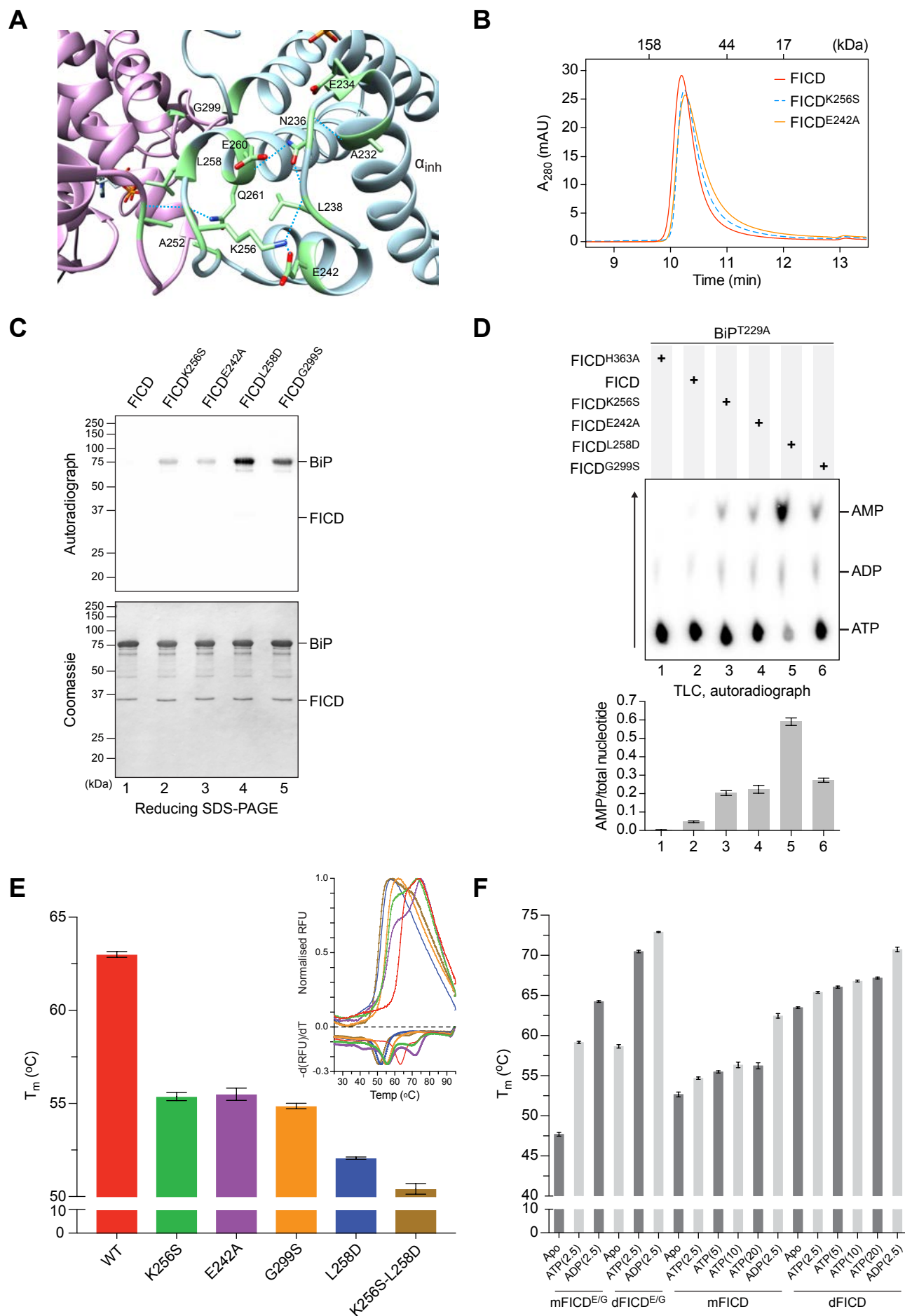


Figure 5

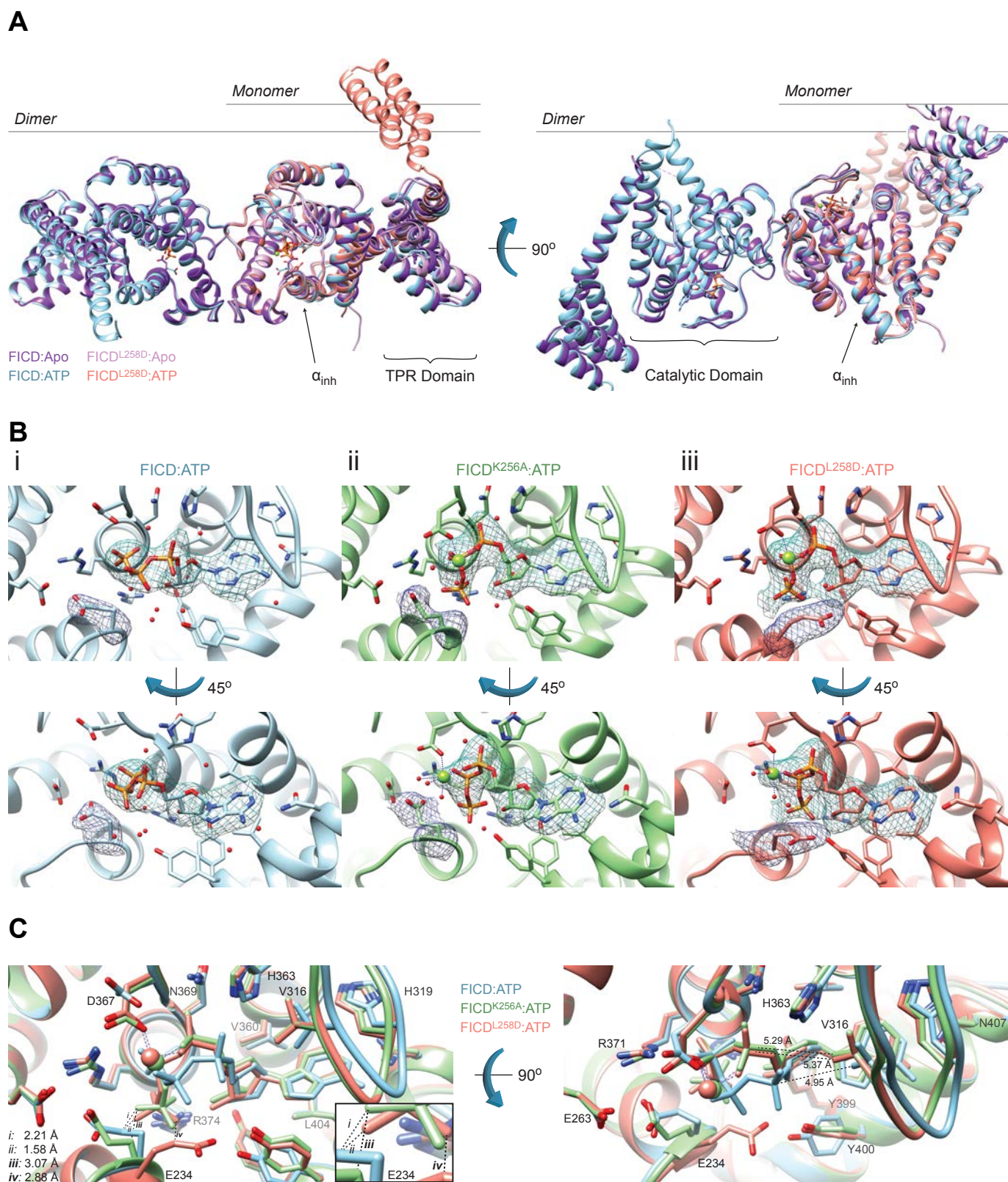


Figure 6

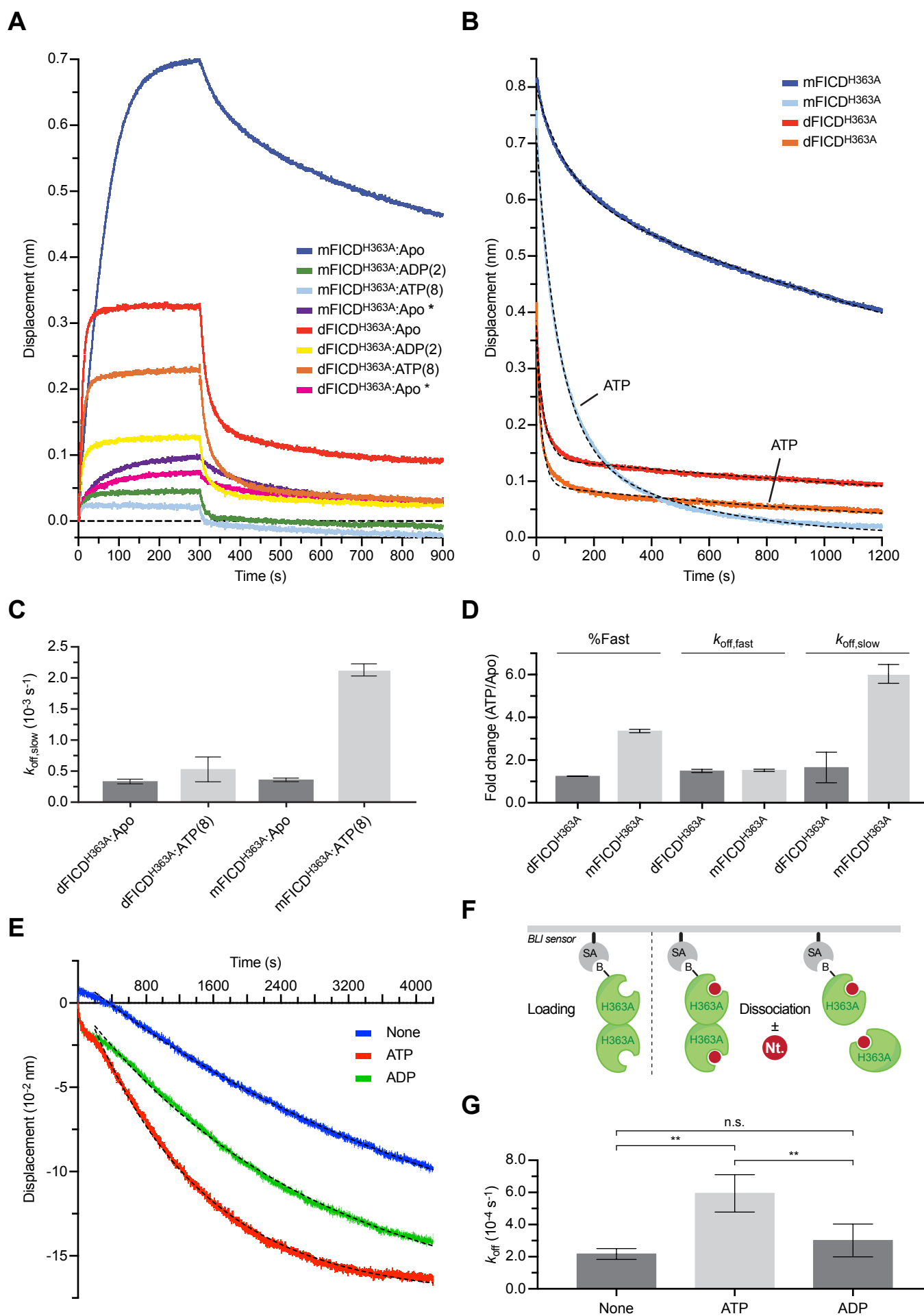


Figure 7

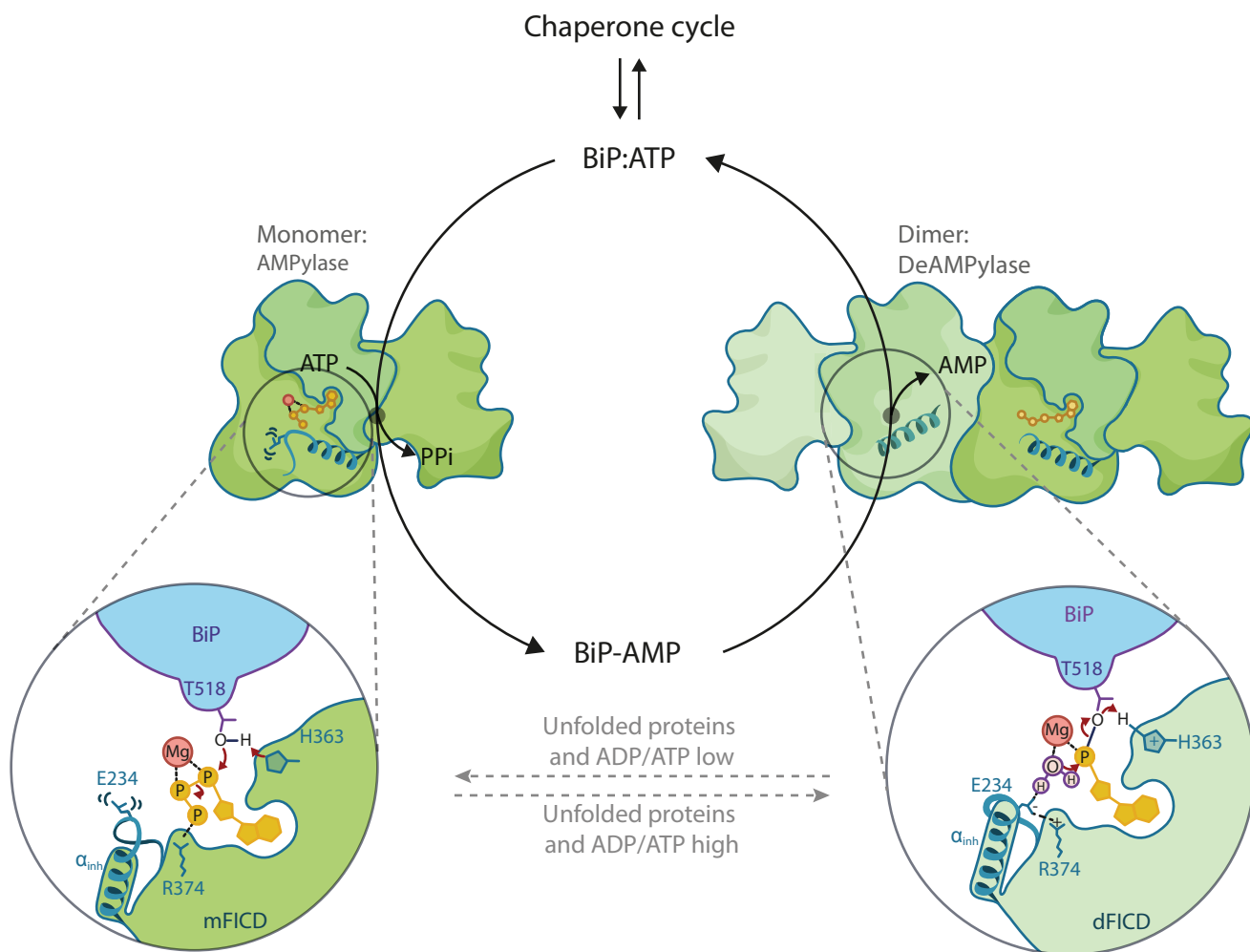


Figure S1

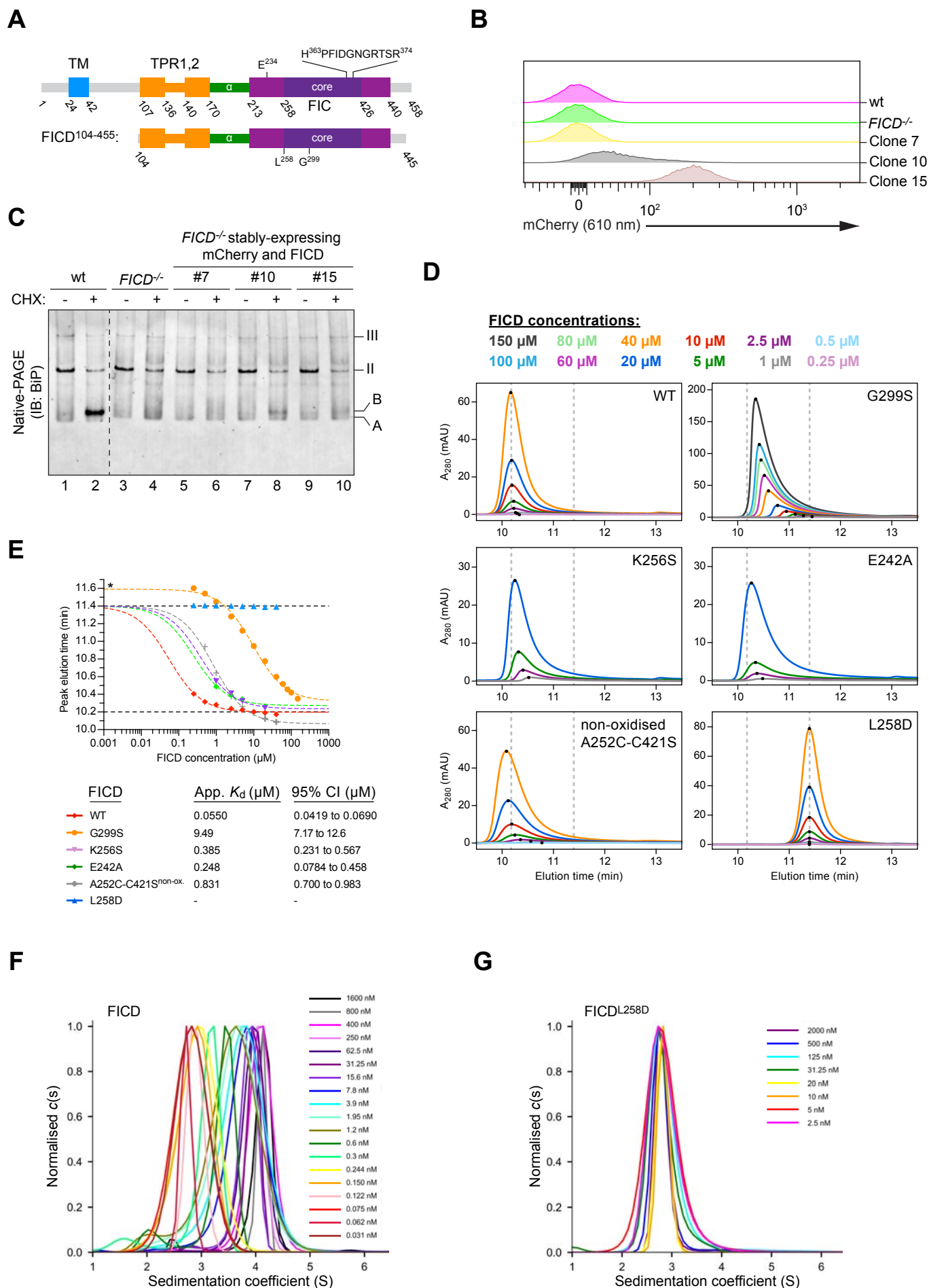


Figure S2

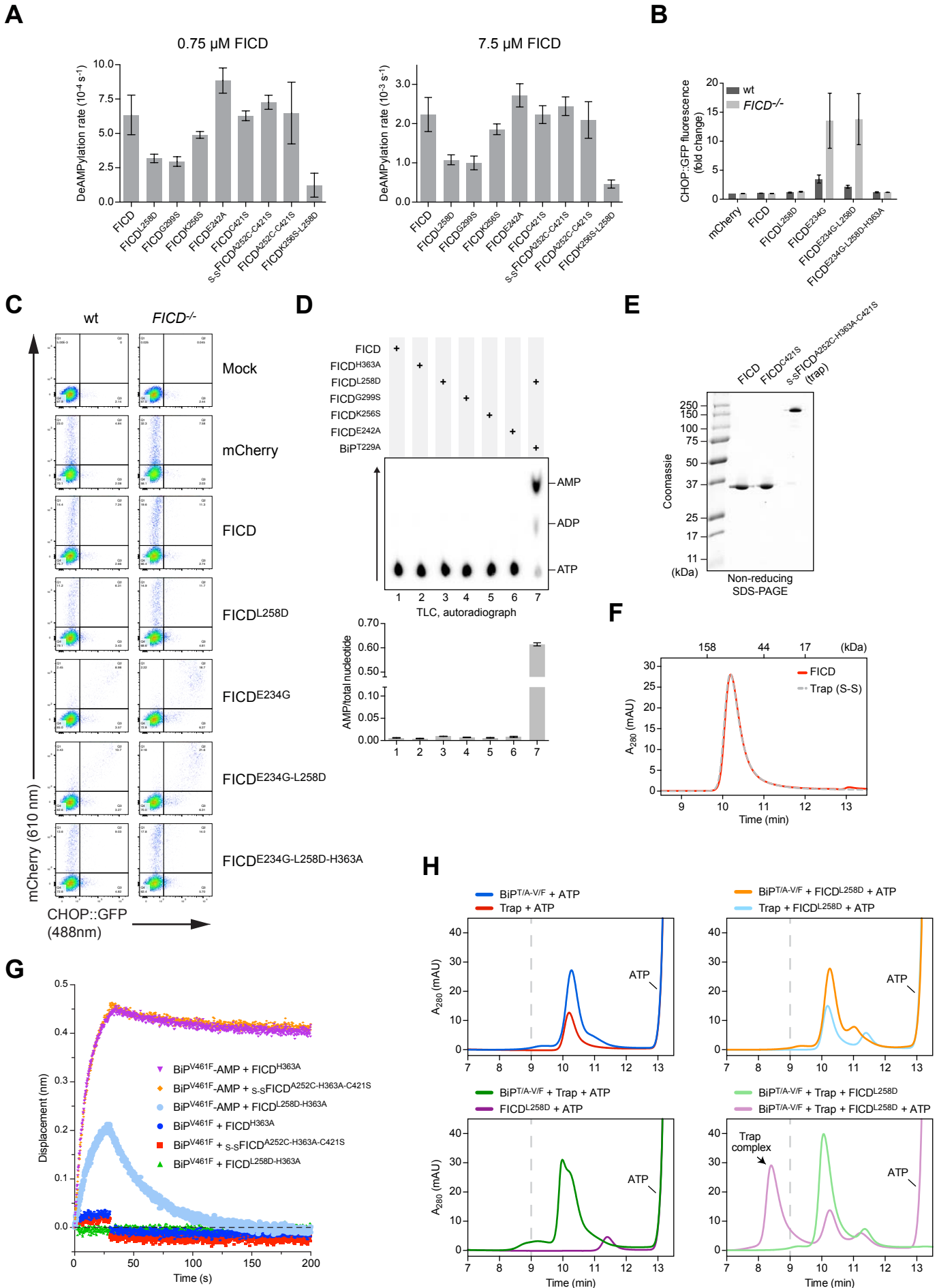


Figure S3

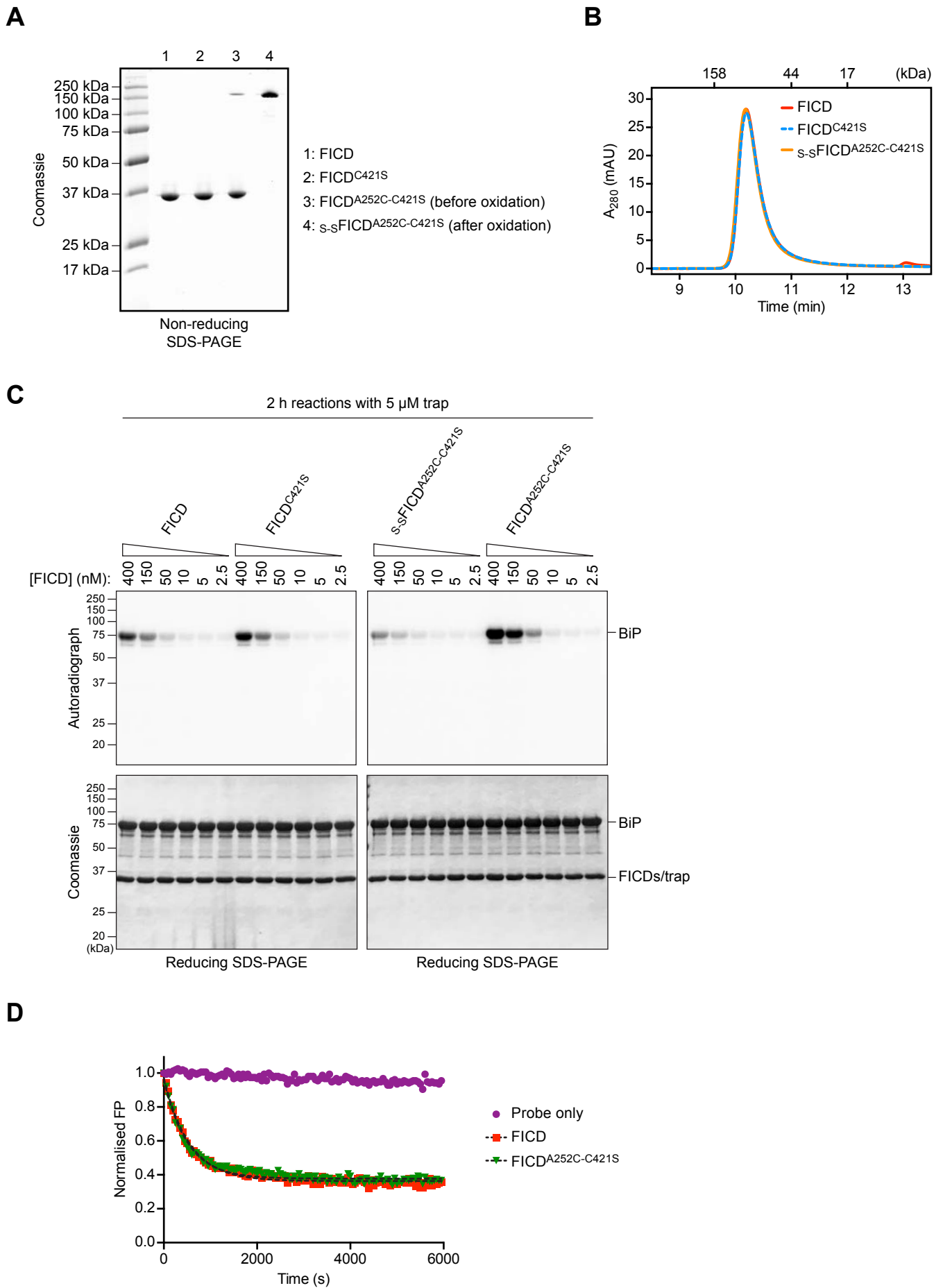


Figure S4

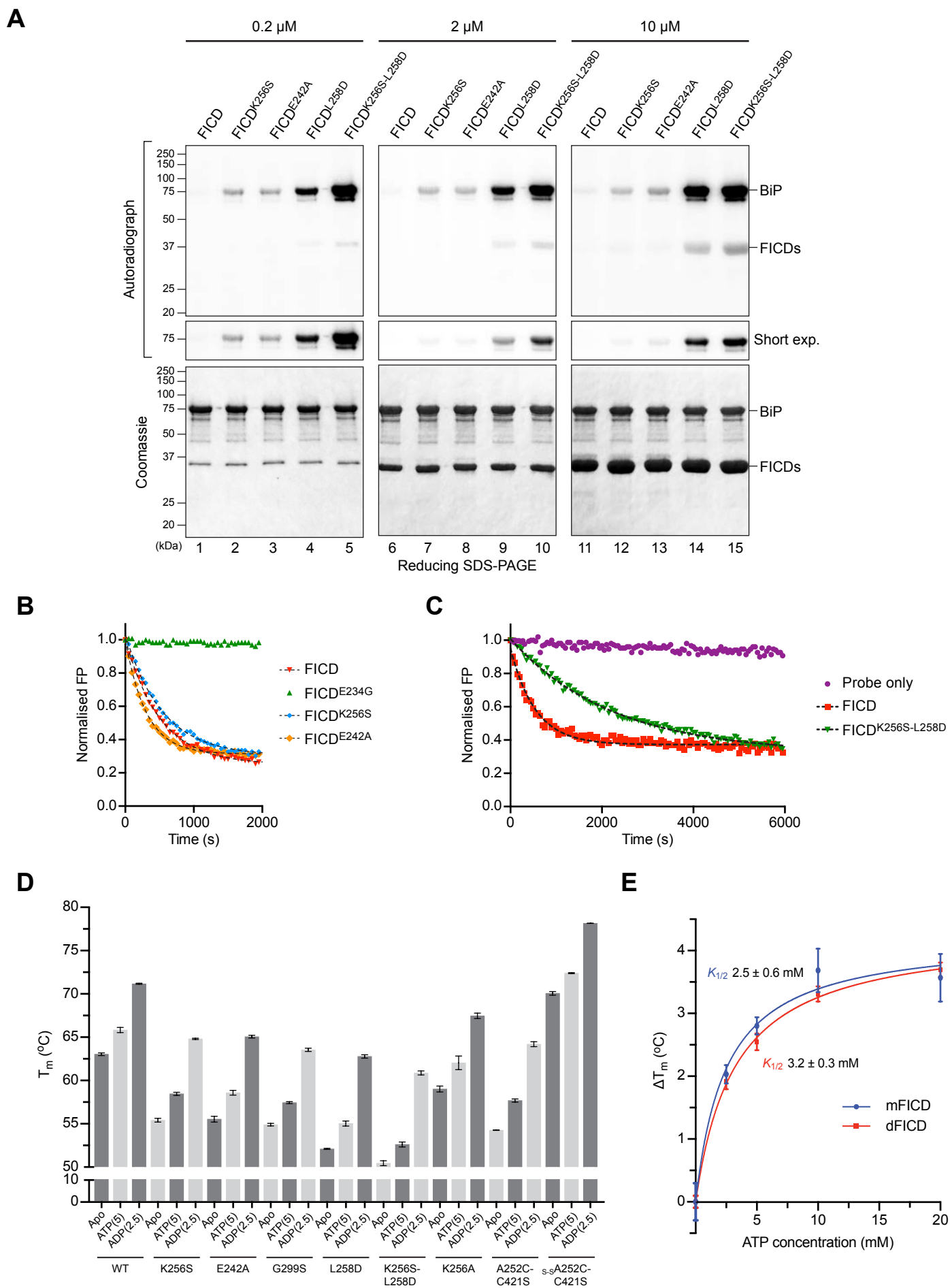


Figure S5

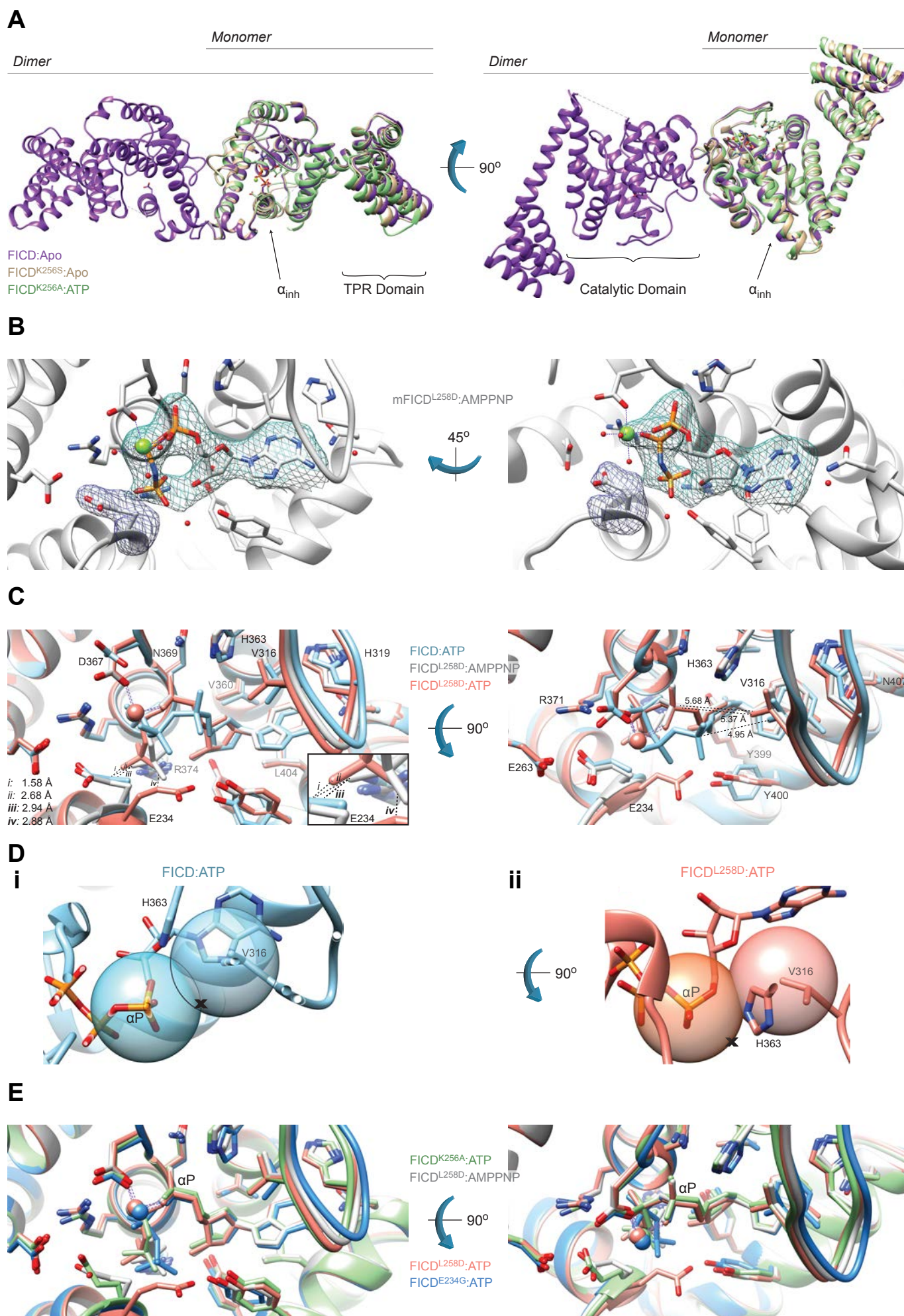


Figure S6

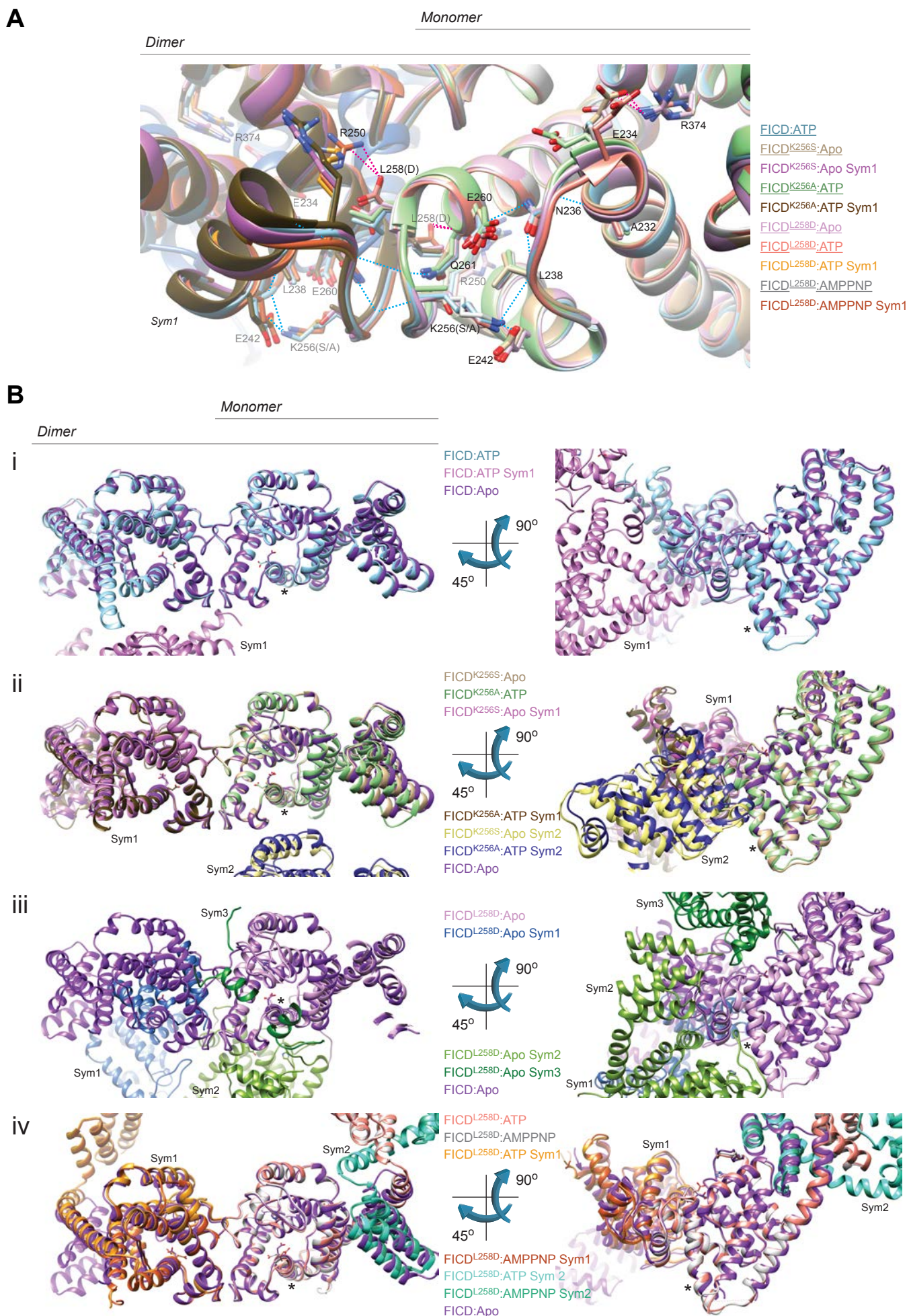


Figure S7

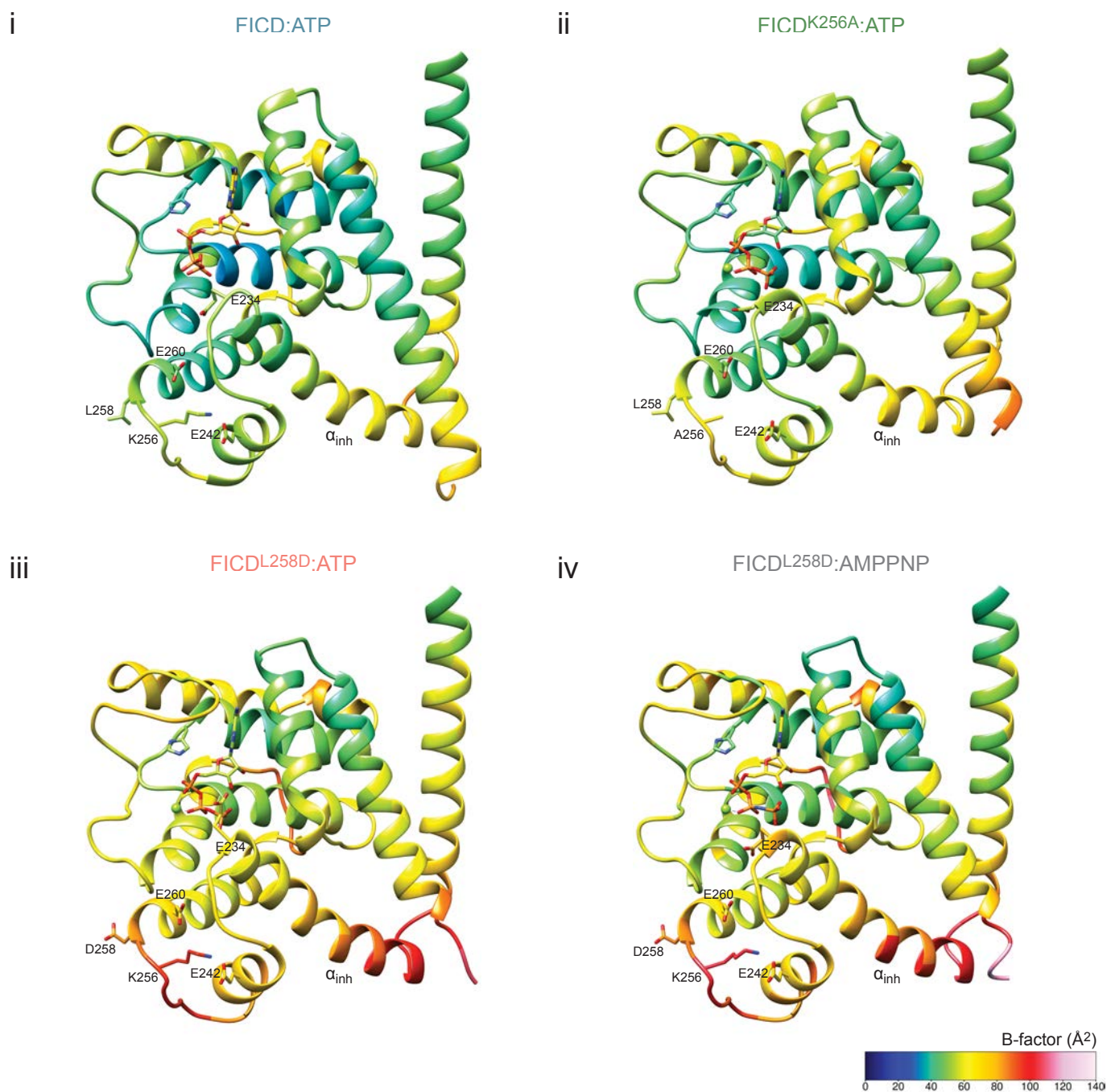


Figure S8

